AECL EACL

CA9600021

AECL-11174, COG-I-94-446

Application of the Integral Method to Modelling the Oxidation of Defected Fuel Elements

Utilisation de la méthode intégrale pour la modélisation de l'oxydation d'éléments combustibles défecteux

Miroslav Kolář

June 1995 juin

AECL

APPLICATION OF THE INTEGRAL METHOD TO MODELLING THE OXIDATION OF DEFECTED FUEL ELEMENTS

by

Miroslav Kolář

Whiteshell Laboratories
Pinawa, Manitoba R0E 1L0
1995

AECL-11174
COG-I-94-446

APPLICATION OF THE INTEGRAL METHOD TO MODELLING THE OXIDATION OF DEFECTED FUEL ELEMENTS

by

Miroslav Kolář

ABSTRACT

Because interim dry storage is an alternative to storage in water pools, it is very important to be able to predict the long-term behaviour of used nuclear fuel in air, especially of fuel elements possibly defected in reactor or during subsequent handling. Extensive oxidation may lead to fuel disintegration and thus to substantially increased costs of interim handling and preparation for final disposal. The ability to predict the extent and rate of oxidation of defected fuel elements under conditions of limited or unlimited oxygen supply would be instrumental in determining the optimum operating conditions of a dry-storage facility.

The starting point for this report is the discrepancy reported in previous work between the reaction-diffusion calculations and the CEX-1 experiment, which involves storage of defected fuel elements in air at 150°C. This discrepancy is considerably diminished here by a more critical choice of theoretical parameters, and by taking into account the fact that different CEX-1 fuel elements were oxidized at very different rates and that the fuel element used previously for comparison with theoretical calculations actually underwent two limited-oxygen-supply cycles. Much better agreement is obtained here between the theory and the third, unlimited-air, storage period of the CEX-1 experiment.

The approximate integral method is used extensively for the solution of the one-dimensional diffusion moving-boundary problems that may describe various storage periods of the CEX-1 experiment. In some cases it is easy to extend this method to arbitrary precision by using higher moments of the diffusion equation.

Using this method, the validity of quasi-steady-state approximation is verified. Diffusion-controlled oxidation is also studied. In this case, for the unlimited oxygen supply, the integral method leads to an exact analytical solution for linear geometry, and to a good analytical approximation of the solution for the spherically symmetric geometry. These solutions may have some application in the analysis of experiments on the oxidation of small UO_2 fragments or powders when the individual UO_2 grains may be considered to be approximately spherical.

AECL
Whiteshell Laboratories
Pinawa, Manitoba R0E 1L0
1995

AECL-11174
COG-I-94-446

UTILISATION DE LA MÉTHODE INTÉGRALE POUR LA MODÉLISATION DE L'OXYDATION D'ÉLÉMENTS COMBUSTIBLES DÉFECTUEUX

par

Miroslav Kolár

RÉSUMÉ

Il est très important de pouvoir prédire le comportement à long terme du combustible nucléaire irradié exposé à l'air, en particulier celui d'éléments combustibles devenus défectueux dans le réacteur ou au cours de leur manutention postérieure, du fait que le stockage provisoire à sec semble être une solution de remplacement économique au stockage provisoire en piscine. Une forte oxydation peut conduire à la désintégration du combustible et ainsi à une augmentation considérable du coût de la manutention intermédiaire et des préparatifs en vue du stockage définitif. La capacité de prédire l'importance et la vitesse d'oxydation des éléments combustibles défectueux dans des conditions d'apport d'oxygène limité ou illimité contribuerait à déterminer les conditions optimales d'exploitation d'une installation de stockage à sec.

Le point de départ du présent rapport est la divergence signalée dans des travaux antérieurs entre les calculs de la réaction-diffusion et l'essai CEX-1, qui porte sur le stockage provisoire d'éléments combustibles défectueux exposés à l'air, à 150 °C. Cette divergence est considérablement restreinte dans ce cas par un choix plus déterminant des paramètres théoriques et en tenant compte du fait que divers éléments combustibles du CEX-1 ont été oxydés à des vitesses très différentes et que l'élément combustible utilisé antérieurement pour la comparaison avec les calculs théoriques a été en réalité soumis à deux cycles d'apport d'oxygène limité. On obtient ici une bien meilleure concordance entre la théorie et les résultats de la troisième période de stockage avec apport d'oxygène illimité de l'essai CEX-1.

La méthode intégrale par approximation est largement utilisée pour résoudre les problèmes de diffusion unidimensionnelle à frontière mobile qui peuvent correspondre à diverses périodes de stockage de l'essai CEX-1. Dans certains cas, il est facile d'étendre cette méthode pour obtenir une précision arbitraire en se servant de moments d'ordre supérieur de l'équation de diffusion.

Cette méthode permet de vérifier la validité de l'approximation de l'état quasi stationnaire. En outre, on étudie l'oxydation régie par la diffusion. Dans ce cas, où l'apport d'oxygène est illimité, la méthode intégrale conduit à une solution analytique précise de la géométrie linéaire et à une bonne approximation analytique de la solution de la géométrie à symétrie sphérique. Ces solutions pourraient trouver quelque application en analyse des essais d'oxydation de petits fragments ou de poudres d'UO_2, lorsque l'on peut considérer que les grains d'UO_2 pris individuellement sont à peu près sphériques.

EACL
Laboratoires de Whiteshell
Pinawa (Manitoba) R0E 1L0
1995

AECL-11174
COG-I-94-446

CONTENTS

1. INTRODUCTION

The stimulation for this study came from the need to predict the long-term behaviour of defected used-fuel elements stored in an interim dry-storage facility. This need is also the motivation behind the long-term Controlled Environment Experiment, Phase 1 (CEX-1), in which a large number of intentionally defected and control undefected irradiated CANDU fuel elements are stored in dry air at 150°C [1, 2]. During the first two CEX-1 storage periods, extending over a total of 99.5 months, the pressure vessel storing the fuel bundles was sealed so that only a limited amount of oxygen was available for oxidation. Because this may not correspond to the situation occurring in commercial dry-storage facilities, unlimited air supply was allowed during the third storage period of 40 months.

The main purpose of this report is to investigate a selection of models that may be applicable to various storage periods of the CEX-1 experiment. We assume that at 150°C the oxidation of UO_2 stops at the approximate composition U_3O_7, although traces of higher uranium oxides (U_3O_8) were found even at this temperature in some specimens recovered after the third storage period.

We start from the discrepancy between theory and experiment reported by Garisto [3]. In Section 2 we review some of the reaction-diffusion models used in Ref. [3], and study the effects of transient processes that were not discussed there in detail, probably because of difficulties with numerical integration in the case of a moving boundary. Here we avoid these numerical problems and independently confirm the theoretical results of Garisto [3] by attacking the moving-boundary problem from a different direction, using the simple integral method [4-6] in which the diffusion equation is satisfied only on average. We show that in some cases this method can be made arbitrarily precise by requiring that an arbitrary number of higher moments of the diffusion equation be satisfied. This approach was suggested in Ref. [5], but does not appear to have been used in actual calculations before. In this way we convert a partial differential equation into a set of ordinary differential equations.

For simplicity, we are studying one-dimensional (1D) models only. This seems to result in errors involving a factor of only 2 in comparison with 2D solutions (representing 3D models with rotational symmetry) [3], whereas the discrepancy between theory and experiment reported by Garisto [3] involves a factor of 170. In any case, enough quantitative experimental data are not available at present for comparison with more exact models. Only "zero-order" reaction in the oxygen concentration is studied, which seems to be justified by the results in Section 3.3. Rigorous treatment of the variable rate of oxygen consumption is presented in Section 2.4 for three different simple types of consumption-rate dependence on the degree of oxidation.

In Section 3 we apply the integral method to diffusion-controlled oxidation, both in linear and spherical geometries. For unlimited oxygen supply in the linear geometry (i.e., in a rod shape) we found an exact solution. This solution also serves for finding a good approximation for the spherical geometry, which can be useful in interpreting some

experiments on the oxidation of individual UO_2 grains. For limited oxygen supply in a fuel rod, infinite time seems to be needed to use up all oxygen trapped in a container.

For unlimited oxygen supply we found that, for the parameter values corresponding to the UO_2 fuel, the time dependence of the advance of the oxidation front through the fuel element is essentially the same in the diffusion-controlled and the reaction-diffusion models. This may be surprising at first glance, until one realizes that at larger times the two models converge, in a sense, as discussed in Section 3.1.

In Section 4 we present a more detailed discussion of some of our calculations and compare them with various experimental data. We arrive at plausible values of the consumption rate and the apparent diffusivity, which give fairly good agreement of theoretical predictions with the CEX-1 data. An independent experimental confirmation of these values, especially of the apparent diffusivity, is desirable.

Finally, Section 5 contains some concluding remarks.

2. REACTION–DIFFUSION MODEL

Equivalent porous medium models formulated by Garisto [3] theoretically allow for an arbitrary ratio of the reaction rate and the apparent diffusivity. Garisto, however, encountered problems with the numerical integration of the diffusion-reaction equation in the presence of a moving boundary. Here we try to confirm the theoretical results of Garisto [3] by attacking the problem from a different direction, using the simple integral method [4-6] in which the diffusion equation is satisfied only on average.

We consider a simplified case: the oxidation of a cylindrical fuel element of radius b with the Zircaloy cladding completely removed from one of its end caps (thus the defect radius is equal to b). This makes it possible to stay within the 1D approximation. The long axis of the fuel element extends along the positive X axis with the defected end positioned at $X = 0$. For $X < 0$ we assume an atmosphere with an oxygen concentration equal to $C_{ex}(\Theta)$ (C_{ex} may depend on time Θ as oxygen is consumed in the case of limited oxygen supply). The concentration of oxygen inside the cracks and pores of fuel is $C(X, \Theta)$. The oxidation of the porous UO_2 is a complex process that takes place throughout the solid matrix. We assume that it can be described by the rate, εK_v, of consumption of oxygen in a unit volume of medium, which also accounts for the diffusion of O_2 through the solid matrix (cf. Section 3.4). Here ε is the total fuel porosity, and K_v is independent of C ("zero-order" in C) and depends only on the local degree of oxidation (i.e., on the amount of UO_2 remaining at a given place). Thus K_v depends implicitly on X and Θ, which will be explicitly denoted as $K_v(X, \Theta)$. In this equivalent porous medium approximation, the reaction-diffusion equation to be solved is [3]

$$\frac{\partial C(X,\Theta)}{\partial \Theta} = D_e \frac{\partial^2 C(X,\Theta)}{\partial X^2} - K_v(X,\Theta); \quad C(X,\Theta) > 0, \tag{1}$$

with the initial and boundary conditions

$$C(X,0) = 0 \quad \text{for } X > 0\,,$$

$$C(0,\Theta) = C_{ex}(\Theta) \quad \text{for } \Theta \geq 0\,,$$

$$C_{ex}(0) = C_0\,,$$

$$K_v(X,0) = K_{v0}\,,$$

and additional conditions relating the oxygen flux at $X = 0$ to $C_{ex}(\Theta)$ and $K_v(X,\Theta)$ to the local degree of oxidation. These are discussed later for individual cases. Equation (1) applies only where $C > 0$. D_e in Equation (1) is the apparent diffusion coefficient of O_2 involving the crack tortuosity.

It is beneficial to introduce the following scaling:

$$X = \alpha\, x\,, \quad \alpha = \sqrt{D_e C_0 / K_{v0}}\,, \tag{2}$$

$$\Theta = \beta\, t\,, \quad \beta = C_0 / K_{v0}\,, \tag{3}$$

$$C(X,\Theta) = C_0\, c(x,t)\,. \tag{4}$$

Then x and t are dimensionless position and time, and in these scaled coordinates the equations for the scaled concentration read as follows:

$$\frac{\partial c(x,t)}{\partial t} = \frac{\partial^2 c(x,t)}{\partial x^2} - k(x,t)\,; \quad c(x,t) > 0\,, \tag{5}$$

$$c(x,0) = 0 \quad \text{for } x > 0\,, \tag{6}$$

$$c(0,t) = c_{ex}(t) \quad \text{for } t \geq 0\,, \tag{7}$$

$$c_{ex}(0) = 1\,, \tag{8}$$

$$k(x,0) = 1\,, \tag{9}$$

where

$$k(x,t) = K_v(X,\Theta)/K_{v0}\,, \tag{10}$$

and

$$c_{ex}(t) = C_{ex}(\Theta)/C_0\,. \tag{11}$$

Note that α can be expressed in terms of Garisto's parameter p [3] as

$$\alpha = \frac{b}{\sqrt{p}}\,.$$

2.1 LOCAL DEGREE OF OXIDATION

The local degree of oxidation, $0 \leq d_o(x,t) \leq 1$, is defined such that $d_o = 0$ corresponds to the unoxidized UO_2 and $d_o = 1$ to complete oxidation to U_3O_7. Here we assume that further oxidation of U_3O_7 to higher uranium oxides can be ignored at the temperature of 150°C maintained in the CEX-1 experiment. Oxidation starts at the position x as soon as the oxygen front arrives at x. Let us denote the time of arrival of the front at x by $t_{\rm arr}(x)$. Depending on the type of the model, the oxygen front can reach a maximum and then recede back to the origin passing through the point x at a later time $t_{\rm dep}(x)$ when the oxidation stops at x. Or it can expand forever; then $t_{\rm dep}(x) = \infty$, and the oxygen front is always identical with the oxidation front. Naturally, there can be more complex situations with the oxygen front moving back and forth several times, each time increasing somewhat the local degree of oxidation, but these are not studied here.

Maximum weight gain of a small volume of fuel, dV, located at x is equal to

$$g_M = \rho\, dV\, (1-\varepsilon)\frac{M_O}{6\, M_{\rm f}}\,,$$

where ρ is the density of UO_2, ε is the total crack and pore porosity, $M_O = 32$ is the molecular weight of oxygen, and $M_{\rm f} = 270$ is the molecular weight of UO_2. The actual weight gain at x starts to be nonzero at $t = t_{\rm arr}(x)$, and is given by the time integral of the rate of oxygen consumption,

$$g = dV\, M_O \int_{\Theta_{\rm arr}(\alpha x)}^{\min(\Theta,\Theta_{\rm dep}(\alpha x))} \varepsilon\, K_v(\alpha x, \Theta')\, d\Theta' = dV\, M_O\, \varepsilon\, \beta\, K_{v0} \int_{t_{\rm arr}(x)}^{\min(t,t_{\rm dep}(x))} k(x,\tau)\, d\tau\,.$$

Here $\Theta_{\rm arr}(\alpha x) = \beta\, t_{\rm arr}(x)$, $\Theta_{\rm dep}(\alpha x) = \beta\, t_{\rm dep}(x)$, and $\Theta' = \beta\,\tau$. The local degree of oxidation is then $d_o(x,t) = 0$ for $t < t_{\rm arr}(x)$, and

$$d_o(x,t) = \frac{g}{g_M} = \frac{1}{\Delta} \int_{t_{\rm arr}(x)}^{\min(t,t_{\rm dep}(x))} k(x,\tau)\, d\tau \quad \text{for} \quad t > t_{\rm arr}(x)\,, \tag{12}$$

where

$$\Delta = \frac{\rho\,(1-\varepsilon)}{6\, M_{\rm f}\, \varepsilon\, K_{v0}\, \beta} = \frac{\rho\,(1-\varepsilon)}{6\, M_{\rm f}\, \varepsilon\, C_0}\,. \tag{13}$$

The dimensionless quantity Δ is essentially a constant: the only parameter in Equation (13) that may vary to some extent is C_0. In addition, there may be some uncertainty in the value of the total porosity ε. Assuming $\varepsilon = 0.05$,[†] we have $\Delta = 15048.0$ for normal atmospheric pressure ($C_0 = 8.55 \times 10^{-6}\,\mathrm{mol \cdot cm^{-3}}$) and $\rho = 10.97\,\mathrm{g \cdot cm^{-3}}$.

[†]The total void volume (including cracks, open porosity, pellet end-dishes, axial and diametral pellet/sheath gaps and internal fission gas plenums) has been measured and found to be less than 3.0 mL for a typical irradiated Pickering or Bruce fuel element [7, 8], which corresponds to a porosity of somewhat less than 0.055.

2.2 UNLIMITED OXYGEN SUPPLY AND CONSTANT CONSUMPTION RATE

The constant consumption rate assumption can be justified for short times only, because in reality the reaction must be switched off at the latest when all UO_2 at the given position x is oxidized. The present assumptions correspond to $c_{ex}(t) \equiv 1$ and $k(x,t) \equiv 1$, and Equations (5) and (7) become

$$\frac{\partial c(x,t)}{\partial t} = \frac{\partial^2 c(x,t)}{\partial x^2} - 1\,; \quad c(x,t) > 0\,, \tag{14}$$

$$c(0,t) = 1 \quad \text{for } t \geq 0\,. \tag{15}$$

Then the scaled equations need to be solved only once, and their solution then scaled back to real coordinates and concentrations using Equations (2) to (4). Equations (14) and (15) have the following steady-state solution (cf. Ref. [3]):

$$\begin{aligned} c(x) &= \tfrac{1}{2}(x - \sqrt{2})^2 \quad \text{for } x \leq \sqrt{2} \\ &= 0 \qquad\qquad\quad \text{for } x > \sqrt{2} \end{aligned}\,. \tag{16}$$

Thus in the original coordinates, $X_{max} = \alpha\sqrt{2}$ is the maximum distance where oxygen penetrates. Beyond this distance no oxidation occurs.

Let us now investigate the transient process in which the steady state in Eq. (16) is approached from the initial state in Eq. (6). We use the integral method originally formulated by Goodman [4], roughly along the lines of Ref. [6]. Let us denote by $x_m(t)$ the right end-point of the interval in which $c(x,t) > 0$ at time t. Apparently $x_m(0) = 0$, $x_m(\infty) = \sqrt{2}$,

$$c(x_m(t), t) = 0 \tag{17}$$

and

$$\left(\frac{\partial c}{\partial x}\right)_{x=x_m(t)} = 0\,. \tag{18}$$

Following Crank and Gupta [6], one can derive the following additional conditions for $x_m(t)$:

$$\left(\frac{\partial^2 c}{\partial x^2}\right)_{x=x_m(t)} = 1\,, \tag{19}$$

$$\int_0^{x_m(t)} \frac{\partial c}{\partial t}\, dx = -\left(\frac{\partial c}{\partial x}\right)_{x=0} - x_m(t)\,, \tag{20}$$

$$\left(\frac{\partial^3 c}{\partial x^3}\right)_{x=x_m(t)} = -\dot{x}_m(t)\,, \tag{21}$$

where the overdot represents as usual the time derivative. Equation (19) was obtained by differentiating Equation (17) by t and using Equations (18) and (14). Equation (20)

was obtained by integrating Equation (14) by x from 0 to x_m (this amounts to requiring that the diffusion-reaction equation is satisfied on average only). Equation (21) was obtained by differentiating Equation (18) by t and using Equations (19) and (14).

One can generate an infinite number of further conditions by considering higher moments in Equation (14), as was suggested in Ref. [5]. This consists of multiplying Equation (14) by x^j and integrating from 0 to x_m:

$$\int_0^{x_m} x^j \frac{\partial c}{\partial t}\, dx = -j \int_0^{x_m} x^{j-1} \frac{\partial c}{\partial x}\, dx \; - \; \frac{x_m^{j+1}}{j+1}; \quad j = 1, 2, \ldots \tag{22}$$

Let us now approximate the solution in Equations (14), (6) and (15) by a polynomial of degree n:

$$c(x,t) = 1 + \sum_{i=1}^{n} a_i(t)\, x^i; \quad 0 \le x \le x_m(t)\,. \tag{23}$$

Substituting this into Equations (17) through (21), and the first $n-4$ equations (22) ($j = 1, 2, \ldots, n-4$), one can obtain a set of $n+1$ ordinary differential equations for $a_i(t)$ and $x_m(t)$ that is approximately equivalent to the original partial differential equation. As $n \to \infty$, we may even hope to obtain the exact solution. Because in the case studied here c monotonically decreases with x, relatively small values of n already give a satisfactory approximation. We show that three different approximations in Equation (23) with $n = 3$ and $n = 4$ already give practically identical results, indicating that we do not need to increase n any more. These approximations are as follows:

(i) $\underline{n = 3}$. Using the conditions in Equations (17) through (20) gives

$$a_1\, x_m = x_m^2/2 - 3\,,$$

$$a_2\, x_m^2 = 3 - x_m^2\,,$$

$$a_3\, x_m^3 = x_m^2/2 - 1\,,$$

$$\dot{x}_m = 12 \frac{2 - x_m^2}{x_m(x_m^2 + 2)}\,.$$

(ii) $\underline{n = 3}$. Using the conditions in Equations (17), (18), and (21) (ignoring (20)) gives the same first three formulas for a_i in terms of x_m as above, and

$$\dot{x}_m = \frac{6}{x_m^3} - \frac{3}{x_m}\,.$$

(iii) $\underline{n = 4}$. Using all conditions in Equations (17) through (21) gives:

$$a_2\, x_m^2 = x_m^2/2 - 3a_1 x_m - 6\,,$$

$$a_3\, x_m^3 = -x_m^2 + 3a_1 x_m + 8\,,$$

$$a_4\, x_m^4 = x_m^2/2 - a_1 x_m - 3\,,$$

$$\dot{x}_m = \frac{6}{x_m^3}(a_1 x_m - x_m^2 + 4)\,,$$

$$\dot{a}_1 = -\frac{1}{x_m^2}[\dot{x}_m\,(x_m^2 + 2a_1 x_m + 8) + 20\,(a_1 + x_m)]\,.$$

One can see that with increasing n, the resulting equations become more complicated and generally cannot be solved analytically. We solved them numerically, using the fourth-order Runge-Kutta algorithm. There is a slight problem with the initial conditions because $x_m(0) = 0$, and at the same time x_m occurs in the denominators of the above equations, thus $\dot{x}_m(0)$ and $\dot{a}_1(0)$ are infinite. Only for $n = 3$ can one integrate uniquely the above equations from $t = 0$, obtaining for small times $x_m(t) \approx 2\sqrt{6t}$ for case (i) and $x_m(t) \approx \sqrt[4]{24t}$ for case (ii). The numerical integration can then be started at a small $t = t_{\rm init} \approx 0.001$ with $x_m(t_{\rm init})$ given by these approximate formulas. For $n = 4$ it is not clear what the best initial condition for a_1 is. At first we tried to derive the initial approximation for $c(x,t)$ from the solution of the reactionless diffusion equation, which is equal to $c(x,t) = \mathrm{erfc}(x/2\sqrt{t}) \approx 1 - \frac{x}{\sqrt{\pi t}} + O((x/\sqrt{t})^3)$. Retaining only the linear part of this solution gives $x_m = \sqrt{\pi\, t_{\rm init}}$, $a_1 = -1/x_m$. After some experimentation, we found that a better starting point (giving results independent of $t_{\rm init}$ as $t_{\rm init} \to 0$) is the one taken from case (i), i.e., $x_m = 2\sqrt{6\, t_{\rm init}}$, and $a_1 = x_m/2 - 3/x_m$.

The dependence of x_m on t obtained in this way for the above three cases is shown in Figure 1. One can see that the limiting value $x_m = \sqrt{2}$ is obtained very rapidly in about one scaled time unit. For the literature values used in Ref. [3], $D_e = 0.2\ \mathrm{cm^2 \cdot s^{-1}}$, $C_0 = 8.6 \times 10^{-6}\ \mathrm{mol \cdot cm^{-3}}$, and $K_{v0} = 4.0 \times 10^{-10}\ \mathrm{mol \cdot cm^{-3} \cdot s^{-1}}$ for 150°C, one gets $\alpha = 65$ cm and $\beta = 21156$ s. That means that the maximum oxygen penetration of $65\sqrt{2}$ cm is achieved in about 6 h; thus the quasi-steady-state approximation used in Ref. [3] is well justified for the range of parameter values considered here.

2.3 LIMITED OXYGEN SUPPLY AND CONSTANT CONSUMPTION RATE

Let us assume that there are N_d *identical* defected fuel elements in a hermetically sealed container. Part of the inner volume of the container, equal to V, is occupied by air. Total influx of oxygen into one defected fuel element is equal to

$$F_{\rm ex} = -\pi b^2 \left(\frac{\partial c}{\partial x}\right)_{x=0} \frac{\varepsilon\, D_e\, C_0}{\alpha}\,, \tag{24}$$

where ε is the total porosity of fuel. The decrease of the external concentration of oxygen is determined by the equation

$$\frac{1}{\beta}\frac{d}{dt}\,(V C_0 c_{\rm ex}) = -N_d\, F_{\rm ex}\,. \tag{25}$$

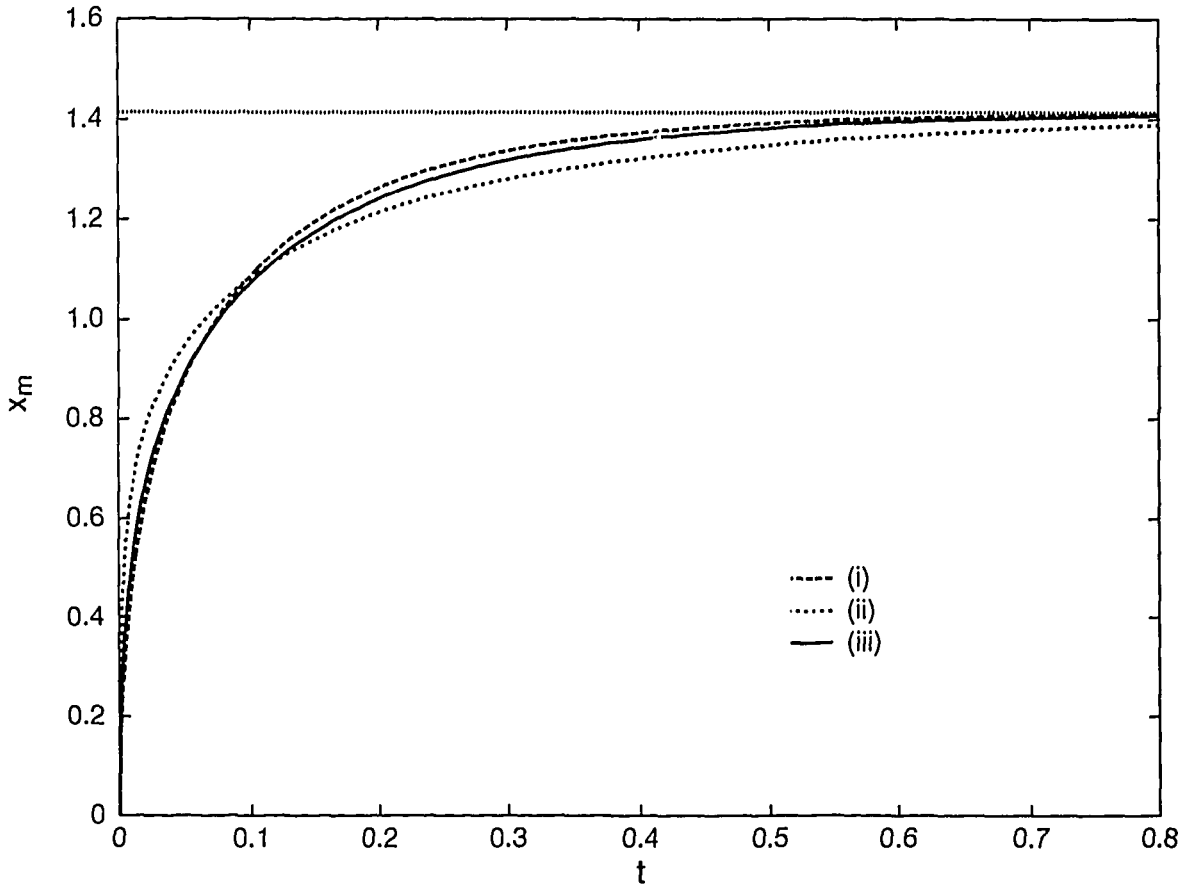

FIGURE 1: The dependence of the maximum oxygen penetration, x_m, on time for $c_{ex} \equiv 1$ and $k \equiv 1$ as obtained by the integral approximations (i), (ii), and (iii) of Section 2.2. The horizontal dotted line corresponds to the limit value of x_m equal to $\sqrt{2}$.

Using Equations (2) and (3), one gets from Equations (24) and (25) the relation

$$\dot{c}_{ex} = P \left(\frac{\partial c}{\partial x} \right)_{x=0} , \tag{26}$$

where

$$P = \pi b^2 \frac{\varepsilon N_d}{V} \sqrt{\frac{D_e C_0}{K_{v0}}} = \frac{\varepsilon}{V} \pi b^2 N_d \, \alpha \, . \tag{27}$$

Note that this quantity is different from p of Ref. [3]. For the time being let us still assume that $k(x,t) = 1$, which is justified if the degree of oxidation remains small everywhere.

Within the integral method, one has now to satisfy simultaneously Equations (14), (6), (7), (8), (26) and a suitable subset of Equations (17) through (22). In the previous subsection we found that the $n = 3$ case (i) (requiring that Equation (20) be satisfied)

already gave good results. Using the same degree of approximation for the present case gives

$$
\begin{aligned}
& c(x,t) = \sum_{i=0}^{3} b_i(t)\, x^i\,; \quad 0 \le x \le x_m(t)\,, \\
& b_1\, x_m = x_m^2/2 - 3b_0\,, \\
& b_2\, x_m^2 = 3b_0 - x_m^2\,, \\
& b_3\, x_m^3 = x_m^2/2 - b_0\,, \\
& \dot{b}_0 = -\frac{P}{2x_m}\left(6b_0 - x_m^2\right)\,, \\
& \dot{x}_m = \frac{1}{x_m^2 + 2b_0}\left[P(6b_0 - x_m^2) - \frac{12}{x_m}(x_m^2 - 2b_0)\right]\,.
\end{aligned}
\tag{28}
$$

These equations give no steady state, although on physical grounds the final state is $x_m = b_0 = 0$, corresponding to all oxygen being used up.

Let us compare the time dependence of the oxygen front obtained from Equations (28) with the quasi-steady-state approximation (QSSA) of Garisto [3]. In our scaled coordinates, QSSA assumes that

$$
c(x,t) = \frac{1}{2}\left[x - x_m(t)\right]^2\,; \quad x_m(0) = \sqrt{2}\,.
$$

Thus

$$
b_0^{\mathrm{QSSA}} = \frac{1}{2}\, x_m^2\,, \tag{29}
$$

and Equation (26) gives $\dot{x}_m = -P$, which integrates to

$$
x_m^{\mathrm{QSSA}} = \sqrt{2} - Pt\,. \tag{30}
$$

In Figure 2 we compare the values of x_m and b_0 obtained by Runge-Kutta integration of the last two equations in Equation (28) with those given by the QSSA formulas (Equations (29) and (30)). One can see that for smaller values of P ($P = 5.6 \times 10^{-4}$ in Figure 2c corresponds to the parameter values given at the end of the previous subsection), QSSA is an excellent approximation – its basic assumption that the all-time maximum oxygen penetration equal to $\sqrt{2}$ is achieved almost instantaneously (relative to the duration of the whole process) is well justified. This is still true even for $P = 0.1$ (Figure 2b).

For small values of P, one can thus safely use the QSSA result of Equation (30). Then $t_{\mathrm{arr}}(x) \approx 0$ for all x, and $t_{\mathrm{dep}}(x) = (\sqrt{2} - x)/P$. For the final degree of oxidation after all available oxygen has been used up, one obtains from Equation (12)

$$
d_o(x,\infty) = \frac{1}{\Delta}\, t_{\mathrm{dep}}(x) = \frac{\sqrt{2} - x}{\Delta P}\,. \tag{31}
$$

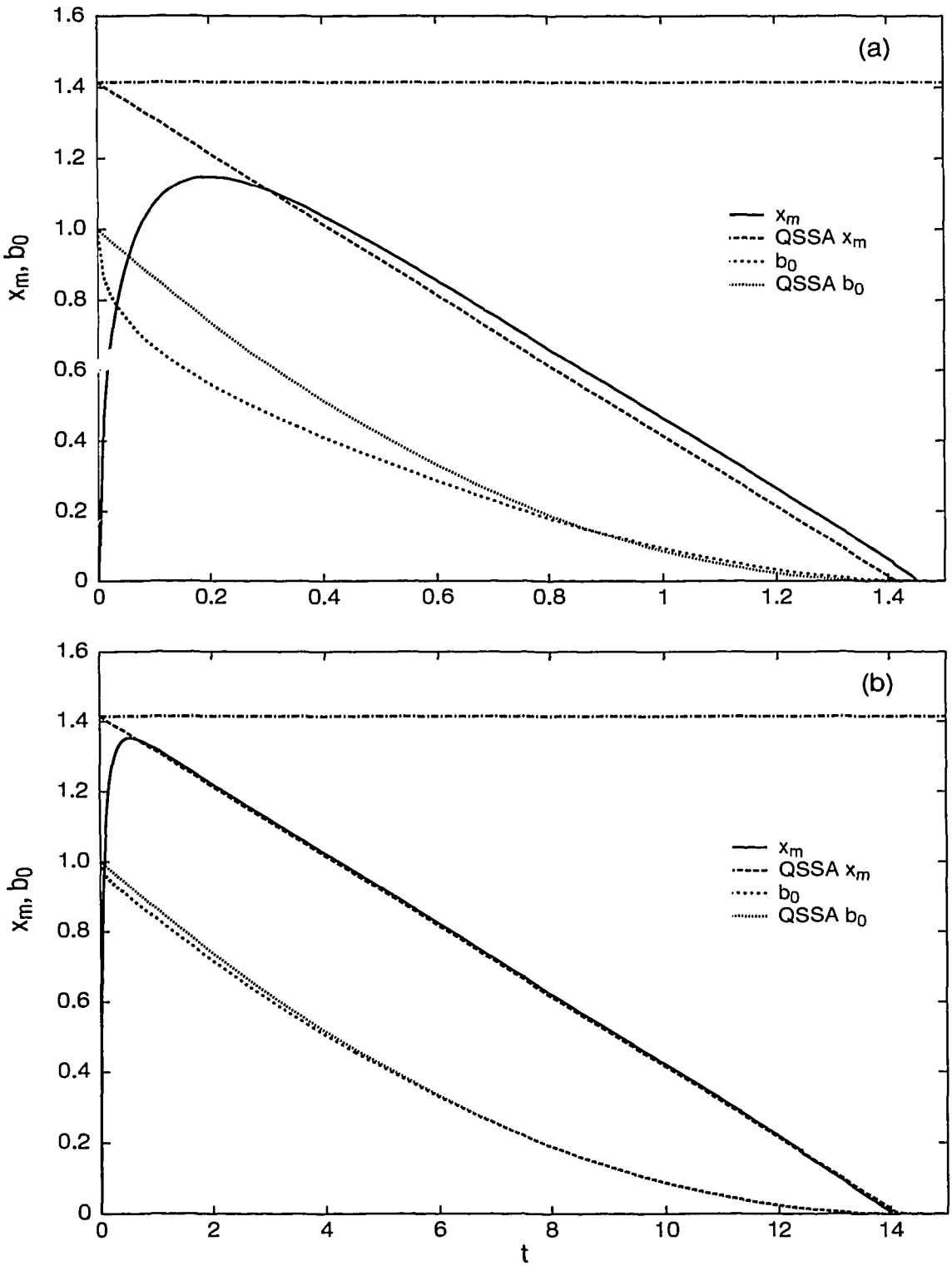

FIGURE 2: The comparison of the maximum oxygen penetration, $x_m(t)$, and the external concentration $c_{ex}(t) \equiv b_0(t)$, obtained by numerical integration of Equations (28) with the QSSA values (Equations (29) and (30)). (a) $P = 1$, (b) $P = 0.1$, and (c) $P = 5.6 \times 10^{-4}$. The dash-dotted horizontal line corresponds to the limit value of x_m equal to $\sqrt{2}$. In plot (c) the exact and QSSA results are practically indistinguishable.

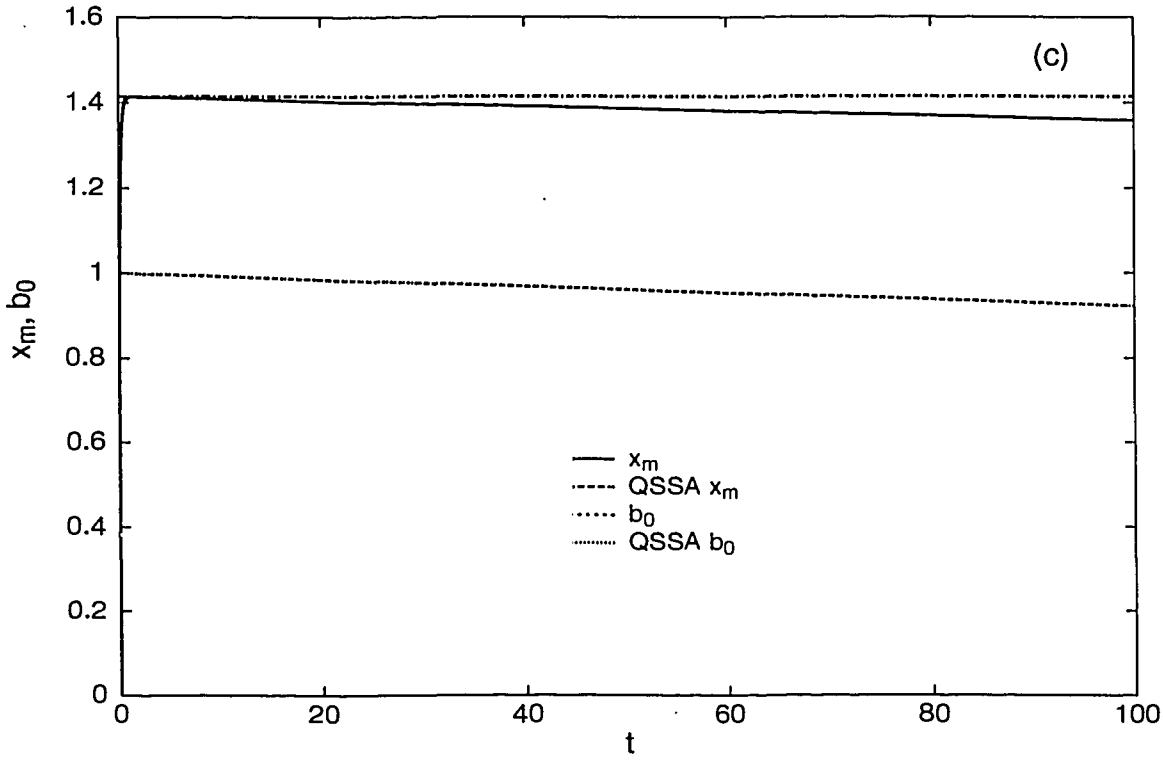

FIGURE 2 continued

Thus the final degree of oxidation decreases linearly with distance from the defect. It is the largest at the defect,

$$d_o(0,\infty) = \frac{\sqrt{2}}{\Delta P} = \frac{6\,M_f\,V}{\rho\,(1-\varepsilon)\,\pi\,b^2\,N_d}\sqrt{\frac{2\,K_{v0}\,C_0}{D_e}}. \tag{32}$$

In real coordinates, the all-time maximum oxygen penetration is

$$X_{\max} = \alpha\sqrt{2} = \sqrt{\frac{2D_e\,C_0}{K_{v0}}}, \tag{33}$$

and the whole process lasts

$$\Theta_{\rm dep}(0) = \frac{V}{\varepsilon\,\pi\,b^2\,N_d}\sqrt{\frac{2C_0}{D_e\,K_{v0}}}. \tag{34}$$

The larger the consumption rate K_{v0}, the shorter the duration of the whole process, the smaller the maximum oxygen penetration, and the higher the degree of oxidation at the surface (defect). Thus the present approximation is not applicable to very large consumption rates when $d_o(0,\infty)$ approaches unity. Then one has to take into account the decrease of the consumption rate with the degree of oxidation. Because in the limited-oxygen-supply storage periods of the CEX-1 experiment, $d_o(0,\infty)$ seems to be below 1, we have not studied here the limited-oxygen-supply case with variable consumption rate.

2.4 UNLIMITED OXYGEN SUPPLY AND VARIABLE CONSUMPTION RATE

In this case $c_{ex}(t) \equiv 1$, and $k(x,t)$ is a suitable function of the local degree of oxidation $d_o(x,t)$ introduced in Section 2.1. Oxidation starts at the position x as soon as the oxygen front, represented by $x_m(t)$, arrives at x. For the unlimited oxygen supply, $x_m(t)$ is always a monotonically increasing function of t, and so the time of arrival, $t_{arr}(x)$, of the oxygen front is given by the inverse of $x_m(t)$:

$$t = t_{arr}(x) \quad \Longleftrightarrow \quad x = x_m(t)\,. \tag{35}$$

In this case $t_{dep}(x) = \infty$. Thus Equation (12) becomes

$$d_o(x,t) = \frac{1}{\Delta} \int_{t_{arr}(x)}^{t} k(x,\tau)\, d\tau \quad \text{for} \quad t > t_{arr}(x)\,. \tag{36}$$

Initially, one always has

$$k(x_m(t),t) \equiv 1\,. \tag{37}$$

For further evolution of $k(x,t)$, let us consider three different model cases of the k versus d_o dependence that are relatively easy to treat semianalytically.

(A) Step-like dependence: $k = 1$ if $d_o < 1$ and $k = 0$ if $d_o = 1$; that is, the rate of oxidation is independent of d_o, but oxidation to U_3O_7 is switched off instantaneously once the fuel is completely oxidized. Then Equation (36) gives

$$d_o(x,t) = \frac{1}{\Delta}\,(t - t_{arr}(x)) \quad \text{if} \quad d_o(x,t) < 1\,, \tag{38}$$

i.e., if $t < t_1(x)$ where $t_1(x)$ is the time when $d_o(x,t)$ reaches the value of 1 at x. Apparently,

$$t_1(x) = t_{arr}(x) + \Delta\,, \tag{39}$$

and

$$k(x,t) = 1 \quad \text{for} \quad t_{arr}(x) \le t < t_1(x)\,, \tag{40}$$

and $k(x,t) = 0$ otherwise.

(B) Linear dependence: $k = 1 - d_o$ while $d_o \le 1$. Then differentiating Equation (36) for this case by t gives

$$\frac{\partial}{\partial t} d_o(x,t) = \frac{1}{\Delta}(1 - d_o(x,t))$$

for $t > t_{arr}(x)$. This differential equation has the solution

$$d_o(x,t) = 1 - e^{-\frac{t - t_{arr}(x)}{\Delta}}\,. \tag{41}$$

Thus

$$k(x,t) = e^{-\frac{t-t_{arr}(x)}{\Delta}}\,, \tag{42}$$

and $t_1(x) = \infty$. Therefore, for this case, the fuel at an arbitrary position x is never completely oxidized in finite time.

(C) Assume that the dependence of k on d_o is such that it gives a linear dependence of k on time:

$$k(x,t) = 1 - w\,[t - t_{arr}(x)]\,, \tag{43}$$

where w is a constant yet to be determined. From Equation (36) one then gets

$$d_o(x,t) = \frac{1}{\Delta}\left[1 + \frac{w}{2}[t_{arr}(x) - t]\right][t - t_{arr}(x)]\,. \tag{44}$$

Equations (43) and (44) must give at time $t = t_1(x)$ simultaneously $k(x,t_1) = 0$ and $d_o(x,t) = 1$. One can satisfy these conditions only if $w = \frac{1}{2\Delta}$ and

$$t_1(x) = t_{arr}(x) + 2\Delta\,. \tag{45}$$

Thus for $t \le t_1(x)$,

$$k(x,t) = 1 - \frac{1}{2\Delta}[t - t_{arr}(x)]\,, \tag{46}$$

$$d_o(x,t) = \frac{1}{\Delta}\left[1 - \frac{1}{4\Delta}[t - t_{arr}(x)]\right][t - t_{arr}(x)]\,. \tag{47}$$

These two equations then give

$$k(x,t) = \sqrt{1 - d_o(x,t)}\,. \tag{48}$$

All three cases are compared in Figure 3. The real situation probably lies somewhere between cases (A) and (C), k at first being independent of time (on d_o), and then rather rapidly going to zero [9-20].

We now attempt to use the integral method to solve Equations (5), (6), and (15). Conditions in Equations (17), (18), and (19) still hold (the last one remains unchanged because of Equation (37)), however Equations (20) and (21) have to be replaced by

$$\int_0^{x_m(t)} \frac{\partial c}{\partial t}\,dx = -\left(\frac{\partial c}{\partial x}\right)_{x=0} - \int_0^{x_m(t)} k(x,t)dx\,, \tag{49}$$

$$\dot{x}_m(t) = -\left(\frac{\partial^3 c}{\partial x^3}\right)_{x=x_m(t)} + \left(\frac{\partial k}{\partial x}\right)_{x=x_m(t)} \tag{50}$$

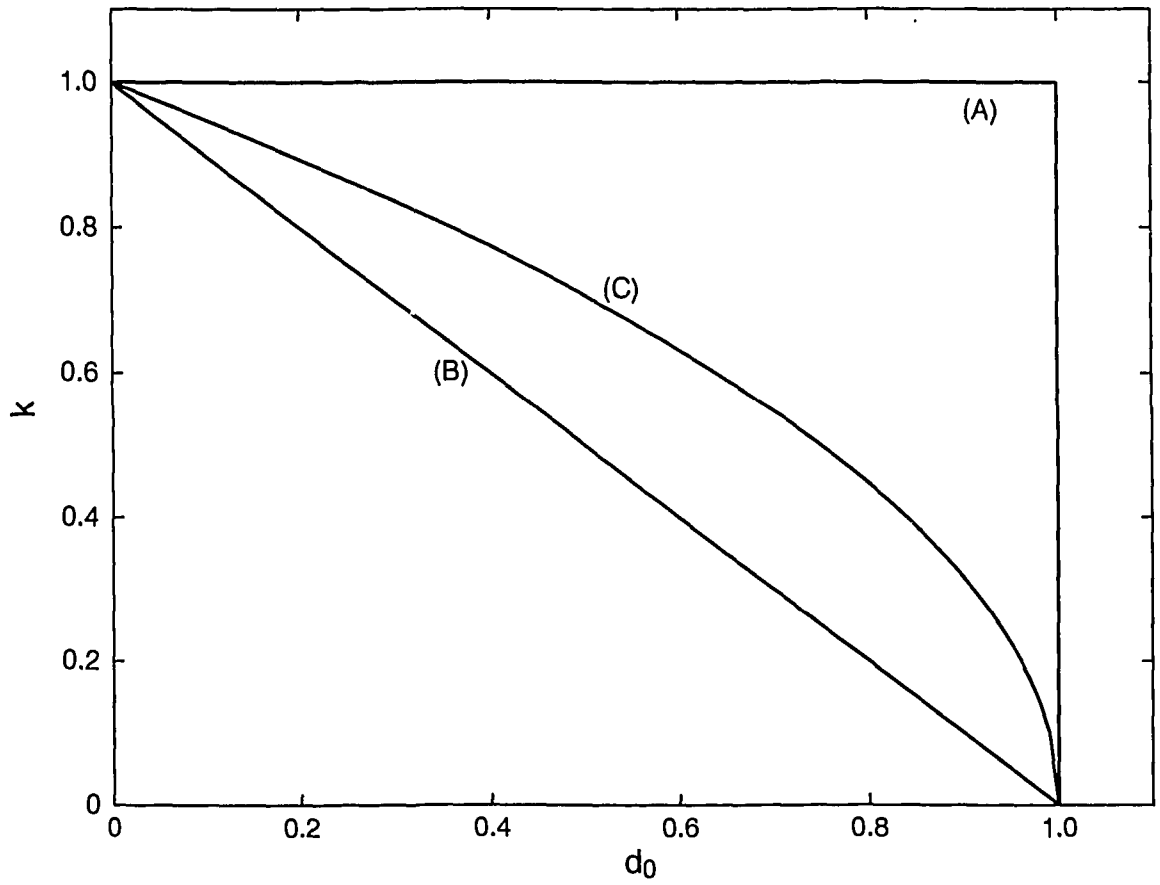

FIGURE 3: The three model dependences of the oxygen consumption rate on the degree of oxidation discussed in Section 2.4.

Let us first calculate the integral that occurs on the right-hand side of Equation (49),

$$I(t) = \int_0^{x_m(t)} k(x,t)dx\,, \tag{51}$$

for the three cases (A), (B), and (C) introduced above.

Case (A). It is apparent that

$$I(t) = x_m(t) - x_{\min}\,,$$

where $x_{\min}$ is the minimum (infimum) of all x such that $d_o(x,t) < 1$, i.e., $t_1(x_{\min}) = t$. Using Equations (39) and (35), one gets $x_{\min} = x_m(t-\Delta)$, and

$$I(t) = x_m(t) - x_m(t-\Delta)\,. \tag{52}$$

Case (B). From Equation (42),

$$I(t) = \int_0^{x_m(t)} \exp\left(-\frac{t - t_{\rm arr}(x)}{\Delta}\right)dx\,.$$

Using substitution $\tau = t_{\rm arr}(x)$, i.e., $d\tau = \frac{dt_{\rm arr}(x)}{dx}dx = \left(\frac{dx_m(\tau)}{d\tau}\right)^{-1} dx$ gives

$$I(t) = \int_0^t \frac{dx_m(\tau)}{d\tau} \exp\left(-\frac{t-\tau}{\Delta}\right) d\tau\,,$$

and integrating by parts finally gives

$$I(t) = x_m(t) - \Phi_{\rm B}(t)\,, \tag{53}$$

where

$$\Phi_{\rm B}(t) = \frac{1}{\Delta}\int_0^t x_m(\tau) \exp\left(-\frac{t-\tau}{\Delta}\right) d\tau\,.$$

Differentiating this formula by t gives

$$\frac{d}{dt}\Phi_{\rm B}(t) = \frac{1}{\Delta}\left[x_m(t) - \Phi_{\rm B}(t)\right]\,; \quad \Phi_{\rm B}(0) = 0\,. \tag{54}$$

Case (C). From Equation (46) we have

$$I(t) = \int_{x_{\rm min}}^{x_m(t)} \left[1 - \frac{1}{2\Delta}\left(t - t_{\rm arr}(x)\right)\right] dx\,,$$

where $x_{\rm min}$ has the same meaning as in case (A) but now $x_{\rm min} = x_m(t-2\Delta)$ by Equation (45). Using the same substitution, $\tau = t_{\rm arr}(x)$, as in case (B) followed again by integration by parts gives

$$I(t) = x_m(t) - \Phi_{\rm C}(t)\,, \tag{55}$$

where

$$\Phi_{\rm C}(t) = \frac{1}{2\Delta}\int_{t-2\Delta}^{t} x_m(t)\, d\tau\,.$$

Here we assume that $x_m(t) = 0$ for $t < 0$. Again, differentiating by t gives

$$\frac{d}{dt}\Phi_{\rm C}(t) = \frac{1}{2\Delta}\left[x_m(t) - x_m(t-2\Delta\right]\,; \quad \Phi_{\rm C}(0) = 0\,. \tag{56}$$

Defining

$$\Phi_{\rm A}(t) = x_m(t-\Delta)\,, \tag{57}$$

one can formally write Equation (49) in all three cases in the same form,

$$\int_0^{x_m(t)} \frac{\partial c}{\partial t}\, dx = -\left(\frac{\partial c}{\partial x}\right)_{x=0} - x_m(t) + \Phi_{\rm case}(t)\,; \quad {\rm case} = {\rm A, B, C}\,, \tag{58}$$

where $\Phi_{\text{case}}(t)$ is given by Equations (57), (54), or (56).

Let us now turn to Equation (50). From Equations (40), (42), or (46) we have

$$\left(\frac{\partial k}{\partial x}\right)_{x=x_m(t)} = f_{\text{case}} \frac{1}{\dot{x}_m(t)\,\Delta}; \quad \text{case} = \text{A, B, C}, \tag{59}$$

where

$$f_{\text{A}} = 0, \quad f_{\text{B}} = 1, \quad f_{\text{C}} = \frac{1}{2}.$$

Here we have made use of Equation (37) for the (B) case.

Let us again assume that the approximation in Equation (23) holds. We investigate the two simplest cases, $n = 3$ and $n = 4$, first.

(I) n=3. Using the conditions in Equation (17), (18), (19), and (58), one obtains the same formulas for a_i in terms of x_m as in case (i) of Section 2.2, and

$$\dot{x}_m = \frac{4}{x_m^2 + 2}\left[\frac{3}{x_m}(2 - x_m^2) + 2\Phi_{\text{case}}\right], \tag{60}$$

where Φ_{case} is given by Equation (57), (54), or (56). Thus in case (A), one has a single differential equation (60); in the other two cases, one has a system of two ordinary differential equations for x_m and Φ_{B} or Φ_{C}. However, for a numerical integration, case (B) is the simplest one because one deals only with quantities related to the same time instant, whereas cases (A) and (C) require storing past values of x_m, at $t - \Delta$ and $t - 2\Delta$ respectively, which makes it very difficult to use an integrating scheme with variable step.

(II) n=4. Using the conditions in Equations (17), (18), (19), (58) and (50) with Equation (59), one obtains the same formulas for a_2, a_3, and a_4 in terms of a_1 and x_m as in case (iii) of Section 2.2, and

$$\dot{a}_1 = -\frac{1}{x_m^2}[\dot{x}_m\,(x_m^2 + 2a_1x_m + 8) + 20\,(a_1 + x_m - \Phi_{\text{case}})], \tag{61}$$

and

$$\dot{x}_m = \frac{6}{x_m^3}(a_1x_m - x_m^2 + 4) \tag{62}$$

in case (A) and

$$\dot{x}_m = \frac{3}{x_m^3}(a_1x_m - x_m^2 + 4) + \sqrt{9\frac{(a_1x_m - x_m^2 + 4)^2}{x_m^6} + \frac{f_{\text{case}}}{\Delta}} \tag{63}$$

in cases (B) and (C). Again, for cases (A) and (C), one needs to store past values of x_m to be able to calculate Φ_{case}.

Actually, it turns out that one can get quite a good idea about the long time behaviour of the solutions for $n = 3$ and $n = 4$ without doing extensive numerical calculations. In case (A), for $t < \Delta$, for both $n = 3$ and 4, $\Phi_A(t) = 0$ and the solution is exactly the same as that for the constant consumption rate (see Figure 1). Because Δ is of the order of 10^4 scaled time units, $x_m(t)$ may be considered constant (equal to $\sqrt{2}$) for $0 < t < \Delta$. At $t = \Delta$, $\Phi_A(t)$ changes very rapidly from 0 to $x_m(t - \Delta) \approx \sqrt{2}$, which will be followed by a fast switching of $x_m(t)$ to a new almost constant plateau. A similar switching can be expected at $t = 2\Delta$, 3Δ, ... Thus the solution will have approximately a step-like form:

$$x_m(t) = \gamma_i \sqrt{2} = \text{const}\,, \quad \Phi_A(t) = \gamma_{i-1}\sqrt{2} \quad \text{for} \quad (i-1)\Delta < t < i\Delta\,; \quad i = 1, 2, \ldots, \infty\,.$$

Substituting this ansatz into Equations (60) and (57) (assuming that $\dot{x}_m = 0$ on the plateaus), one gets for γ_i the following recursion relation:

$$\gamma_i = \frac{1}{3}\left(\gamma_{i-1} + \sqrt{\gamma_{i-1}^2 + 9}\right)\,. \tag{64}$$

Starting with $\gamma_1 = 1$, this gives $\gamma_2 = 1.387426$, $\gamma_3 = 1.564239$, $\gamma_4 = 1.649186$, $\gamma_5 = 1.690869$, etc. As $i \to \infty$, γ_i goes to a fixed point $\gamma_\infty = \sqrt{3}$ as can be checked by direct substitution into Equation (64). This corresponds to $x_m(\infty) = \sqrt{6}$. The same steady state can in fact be obtained directly from Equation (60) ($\Phi_A(t) = x_m(t - \Delta) \equiv x_m(t) = \sqrt{6}$).

Similarly for $n = 4$, one gets from Equations (61), (62), and (57)

$$\gamma_i = \frac{1}{4}\left(\gamma_{i-1} + \sqrt{\gamma_{i-1}^2 + 16}\right)\,, \tag{65}$$

and $a_1(t) = (\gamma_{i-1} - \gamma_i)\sqrt{2}$ for $(i-1)\Delta < t < i\Delta$. The values of γ_i are now different, $\gamma_1 = 1$, $\gamma_2 = 1.280776$, $\gamma_3 = 1.370206$, $\gamma_4 = 1.399595$, $\gamma_5 = 1.409346$, etc. The fixed point is now $\gamma_\infty = \sqrt{2}$ giving $x_m(\infty) = 2$ and $a_1(\infty) = 0$. Again, this steady state can be obtained directly from Equations (61) and (62).

Unfortunately, the long time behaviour (the values of the plateaus) and the $t = \infty$ limits are rather different for $n = 3$ and $n = 4$. Evidently, for this problem one has to use higher values of n to achieve convergence. Moreover, the fact that $x_m(\infty)$ (the range of oxidation) is finite does not seem physical. As is shown below, for higher n (satisfying the higher moments of the diffusion-reaction equation), there is no $t = \infty$ steady state, and $x_m(t)$ is unbounded.

For $n = 3$, one can easily check that the (B) and (C) cases give the same $t = \infty$ limit as the (A) case, $x_m(\infty) = \sqrt{6}$.

Numerical integration can be done most easily in the (B) case. For $n = 4$, it indicates that the long-time dependence of x_m, Φ_B and a_1 on time is approximately linear. Equations (61), (63), and (54) really give for $t \to \infty$ an approximate solution in the form

$$x_m(t) \approx \frac{t}{\sqrt{\Delta}}\,, \quad a_1(t) \approx -\frac{t}{3\sqrt{\Delta}}\,, \quad \text{and} \quad \Phi_B(t) \approx \frac{t-\Delta}{\sqrt{\Delta}}\,, \tag{66}$$

which agrees with the numerical results.

Similarly, for the (C) case, one can obtain from Equations (61), (63), and (56) for $t \to \infty$ a similar approximate solution in the form

$$x_m(t) \approx \frac{t}{\sqrt{2\Delta}}, \quad a_1(t) \approx -\frac{t}{3\sqrt{2\Delta}}, \quad \text{and} \quad \Phi_C(t) \approx \frac{t}{\sqrt{2\Delta}}. \tag{67}$$

These limit solutions give monotone $c(x,t)$ for $x_m(t) \lesssim 3.8$. For larger x_m (larger times) a minimum starts to develop in the first half of the interval $(0, x_m)$ and a maximum in the second half. Eventually, the minimum drops below zero and the maximum becomes larger than 1. Thus we again have unphysical behaviour for large times. In summary, in all three cases, (A), (B), and (C), there is a significant difference between the $n = 3$ and $n = 4$ results for long times, and all the long-time results are unphysical in some aspects. To obtain convergence, one has to use larger values of n. For a given n, the value of $c(x,t)$ must equal the exact value in at least $n-4$ points of the interval $(0, x_m)$. Thus as n increases, one can expect that the onset of unphysical behaviour will be delayed to larger times. For large n, one needs an equivalent of the condition in Equation (22) for the present case of the variable consumption rate, which reads

$$\int_0^{x_m} x^j \frac{\partial c}{\partial t}\, dx = -j \int_0^{x_m} x^{j-1} \frac{\partial c}{\partial x}\, dx - \int_0^{x_m} x^j\, k(x,t)\, dx\,. \tag{68}$$

For $j = 1$, this condition must be satisfied by any approximation with $n > 4$. Because for $j = 1$ the first term on the right-hand side of Equation (68) is equal to 1 by Equations (15) and (17), one can immediately see that this condition cannot produce a steady state for $t \to \infty$. In a steady state, $\partial c/\partial t = 0$, thus the left-hand side of Equation (68) would be equal to zero. Similarly, as $x_m(t \to \infty) \to \text{const}$, the integral in the second term on the right-hand side would go to zero for all three cases (A), (B), and (C) because the range of x values where $k(x,t) > 0$ would go to zero. This would lead to a contradiction because of the presence of 1 on the right-hand side of Equation (68) for $j = 1$. Thus the solutions for x_m for $n > 4$ are expected to be continually growing for all times.

Let us denote the last term in Equation (68) by $I_j(t)$, i.e.,

$$I_j(t) = \int_0^{x_m} x^j\, k(x,t)\, dx\,.$$

Following the same procedure as in the case of Equation (51), one gets

$$I_j(t) = \frac{1}{j+1} \left[x_m^{j+1}(t) - \Phi_{j\text{case}}(t) \right],$$

where

$$\Phi_{jA}(t) = x_m^{j+1}(t - \Delta),$$

$$\frac{d}{dt}\Phi_{j\mathrm{B}}(t) = \frac{1}{\Delta}\left[x_m^{j+1}(t) - \Phi_{j\mathrm{B}}(t)\right]\ ; \quad \Phi_{j\mathrm{B}}(0) = 0\,,$$

$$\frac{d}{dt}\Phi_{j\mathrm{C}}(t) = \frac{1}{2\Delta}\left[x_m^{j+1}(t) - x_m^{j+1}(t-2\Delta\right]\ ; \quad \Phi_{j\mathrm{C}}(0) = 0\,.$$

Thus $i(t)$ of Equation (51) is equal to $I_0(t)$ as expected.

Let us assume that Equation (23) holds, and introduce the abbreviation $\bar{a}_i(t) = a_i(t)\,x_m^i(t)$. Then to satisfy Equations (17), (18), (19), (49), (50), and (68), the following relations must hold:

$$1 + \sum_{i=1}^{n} \bar{a}_i(t) = 0\,,$$

$$\sum_{i=1}^{n} i\,\bar{a}_i(t) = 0\,,$$

$$\sum_{i=2}^{n} i(i-1)\,\bar{a}_i(t) = x_m^2(t)\,,$$

$$\sum_{i=1}^{n} \frac{1}{i+1}\left[\dot{\bar{a}}_i\,x_m - i\,\bar{a}_i\,\dot{x}_m\right] = -\frac{\bar{a}_1}{x_m} - x_m + \Phi_{\mathrm{case}}\,, \tag{69}$$

$$\text{case A}: \ \dot{x}_m = -D_3\,; \ \text{ where } \ D_3 = \frac{1}{x_m^3}\sum_{i=3}^{n} i(i-1)(i-2)\bar{a}_i\,,$$

$$\text{case B, C}: \ \dot{x}_m = -\frac{D_3}{2} + \sqrt{\frac{D_3^2}{4} + \frac{f_{\mathrm{case}}}{\Delta}}\,,$$

$$\sum_{i=1}^{n} \frac{1}{i+j+1}\left[\dot{\bar{a}}_i\,x_m - i\,\bar{a}_i\,\dot{x}_m\right] = -j\sum_{i=1}^{n}\frac{i}{i+j-1}\,\frac{\bar{a}_i}{x_m} - \frac{1}{j+1}\left[x_m - \frac{1}{x_m^j}\,\Phi_{j\mathrm{case}}\right]\ ;$$

$$j = 1, \ldots, n-4\,.$$

Again, one can express $\bar{a}_{n-2}$, $\bar{a}_{n-1}$ and $\bar{a}_n$ in terms of the remaining $\bar{a}_i$. Differential equations for the remaining $\dot{\bar{a}}_i$ have the same form for all three cases, and can be obtained from the above relations using the MAPLE V program listed in Appendix A. This program also gives the step-like approximation to their solution in case (A), and the asymptotic behaviour of the solution in the (B) and (C) cases.

In the (A) case, the values of the plateaus are the same for all $n \geq 5$ (the corresponding values of $\bar{a}_i$ were calculated explicitly up to $n = 20$), and are given by the recursive relation

$$\gamma_i = \sqrt{\gamma_{i-1}^2 + 1}\,, \quad \text{which gives} \quad \gamma_i = \sqrt{i}$$

because $\gamma_1 = 1$. This approximate solution is presented in Figure 4. The centres of the plateaus of $x_m(t)$ can be connected by a smooth curve of the form $\sqrt{2\,t/\Delta + 1}$. This

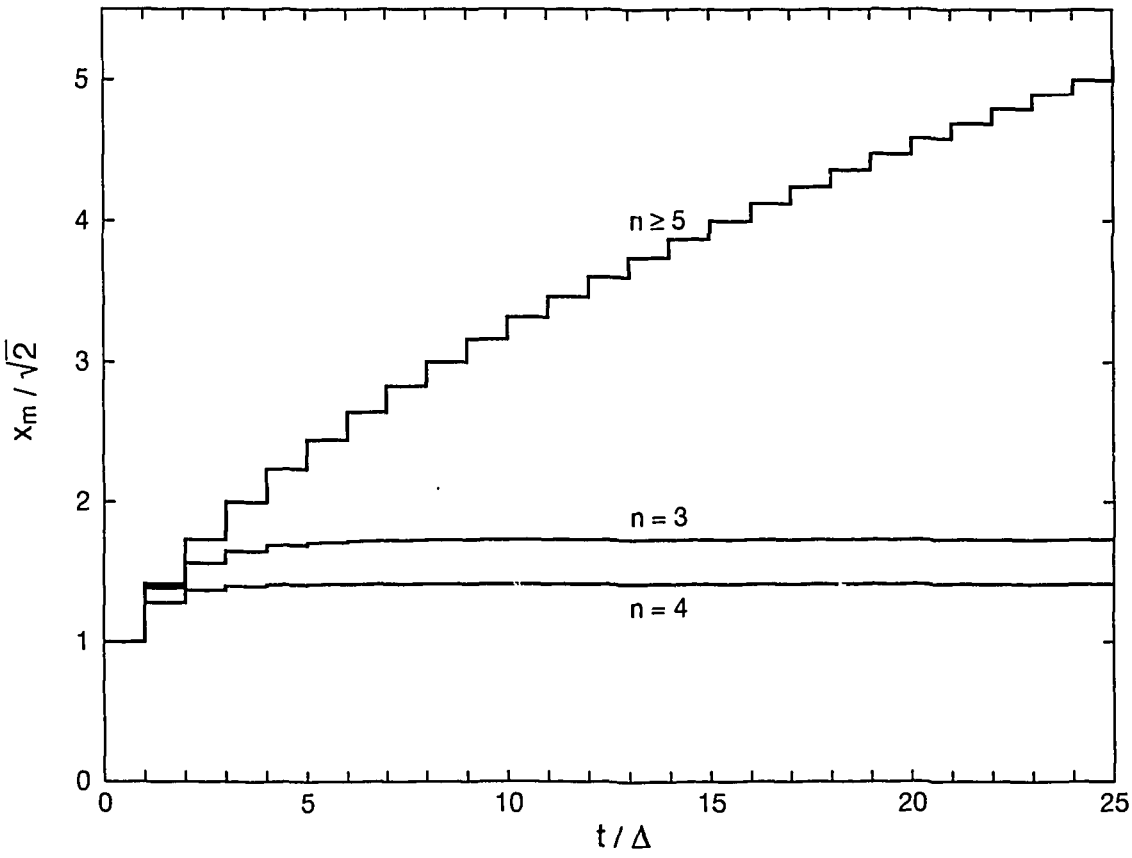

FIGURE 4: Approximate step-like time dependence of the oxidation front for the unlimited oxygen supply and the case (A) dependence of the oxygen consumption rate on the local degree of oxidation. For all $n \geq 5$ the "staircase" is the same.

smooth curve represents a good approximation of the advance of the oxidation front, especially for larger times,

$$x_m(t) \approx \sqrt{\frac{2t}{\Delta}}. \tag{70}$$

In reality, the edges of the steps would be somewhat rounded. In real coordinates, this smooth curve has the equation

$$X_m(\Theta) \approx \alpha \sqrt{\frac{2\Theta}{\beta\Delta}} = \sqrt{\frac{12\, M_f\, \varepsilon\, C_0\, D_e}{\rho\,(1-\varepsilon)}}\, \sqrt{\Theta}. \tag{71}$$

Note that the average advance of the oxidation front does not depend on the consumption rate K_{v0} at all, only on the product $C_0\, D_e$, that is, on the rate of supply of oxygen through the medium. The values of the plateaus are $\sqrt{i}\, X_{\max}$, where $X_{\max}$ is given by Equation (33), and the jumps between successive plateaus occur at time instants equal to the multiples of

$$\beta\Delta = \frac{\rho(1-\varepsilon)}{6 M_f \varepsilon K_{v0}}. \tag{72}$$

Thus as K_{v0} increases, both the step height and the width decrease; however, the centres of the steps will always lie on the same curve (Equation (71)). Let $(i-1)\Delta < t < i\Delta$. Then the local degree of oxidation equals 1 for $x < \sqrt{2(i-1)}$, and for all $\sqrt{2(i-1)} < x < \sqrt{2i}$ it grows practically simultaneously from 0 to 1 as time proceeds from $(i-1)\Delta$ to $i\Delta$; cf. Equation (38).

In the (B) and (C) cases, the MAPLE V program in Appendix A confirmed that the long-time asymptotic behaviour of the solution apparently has, for all $n \geq 4$, the same form as that of Equations (66) and (67); that is,

$$x_m(t) \approx \xi\, t\,, \quad \bar{a}_i \approx \alpha_i\, t^2\,; \quad i = 1, \ldots, n\,, \tag{73}$$

where ξ and α_i are constants. From Equation (69) we again have $\xi = \sqrt{f_{\text{case}}/\Delta}$. For all $n \geq 5$, $\alpha_1 = (-1)^{n-1}\xi^2/(n-1)$; for all $n \geq 6$, $\alpha_2 = (-1)^n(n-1)\xi^2/2$, etc. Thus one can immediately see that the asymptotic behaviour is unphysical at least for all odd n because $\alpha_1 > 0$ for odd n. In fact, it is unphysical for all n, but as n increases, the onset of unphysical behaviour is delayed to larger and larger times, as illustrated in Figures 5 and 6. Figure 5 is for the value of Δ corresponding to UO_2 fuel; Figure 6 is for a much smaller value of Δ to show more easily the asymptotic behaviour of $x_m(t)$. The very-short-time behaviour is the same as that for the constant consumption rate (see Figure 1); that is, x_m "shoots up" from zero practically immediately to $\sqrt{2}$ where it stays for some time. In this initial phase all n (even $n = 3$, cf. Figure 5a) give quite satisfactory results. As the local degree of oxidation near the origin (defect) increases, the oxygen consumption rate starts to decrease in the immediate vicinity of the defect, and x_m slowly starts to increase further. For larger times, the exact x_m then apparently follows the same parabola of Equation (70) that was obtained by smoothing the case (A) "staircase" of Figure 4. Actually, the exact $x_m(t)$ can in case (B) be approximated much better – almost exactly, immediately from $t = 0$ by a shifted parabola

$$x_m(t) = \sqrt{2 + \frac{2\,t}{\Delta}} \tag{74}$$

or

$$X_m(\Theta) = \sqrt{X_{\max}^2 + \frac{12\, M_f\, \varepsilon\, C_0\, D_e}{\rho\,(1-\varepsilon)}\,\Theta}\,. \tag{75}$$

Because the asymptotic behaviour of $x_m(t)$ corresponding to a finite n is linear (cf. Equation (73) and Figure 6b), no finite n can follow this parabola for all times. As n increases, the approximate x_m leaves the parabola at ever increasing times (compare $n = 4$ and $n = 5$ in Figures 5 and 6). Thus the time interval in which a finite-n approximate solution represents correctly the exact one, increases with n.

Although we have not proved it rigorously yet, our results nevertheless indicate convincingly that in case (B) the exact time dependence of the oxidation front is given by Equation (74) or (75), which for large times are exactly the same as the smoothed

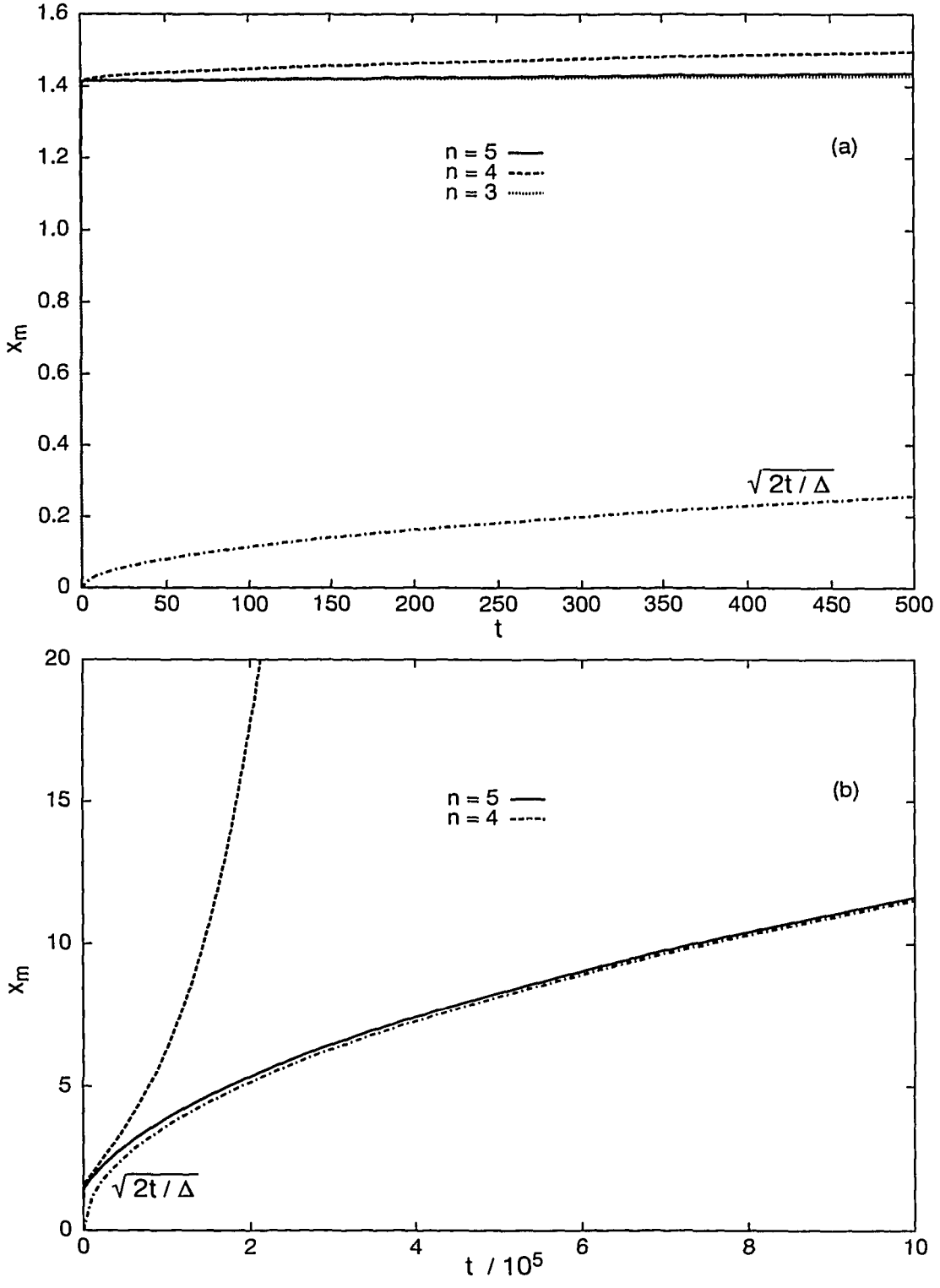

FIGURE 5: The time dependence of the oxidation front for the unlimited oxygen supply and the case (B) dependence of the oxygen consumption rate on the local degree of oxidation for a few lowest n compared with the curve $\sqrt{2\,t/\Delta}$ (representing the smoothed case (A) time dependence). $\Delta = 15048$. (a) is the enlarged initial portion of (b).

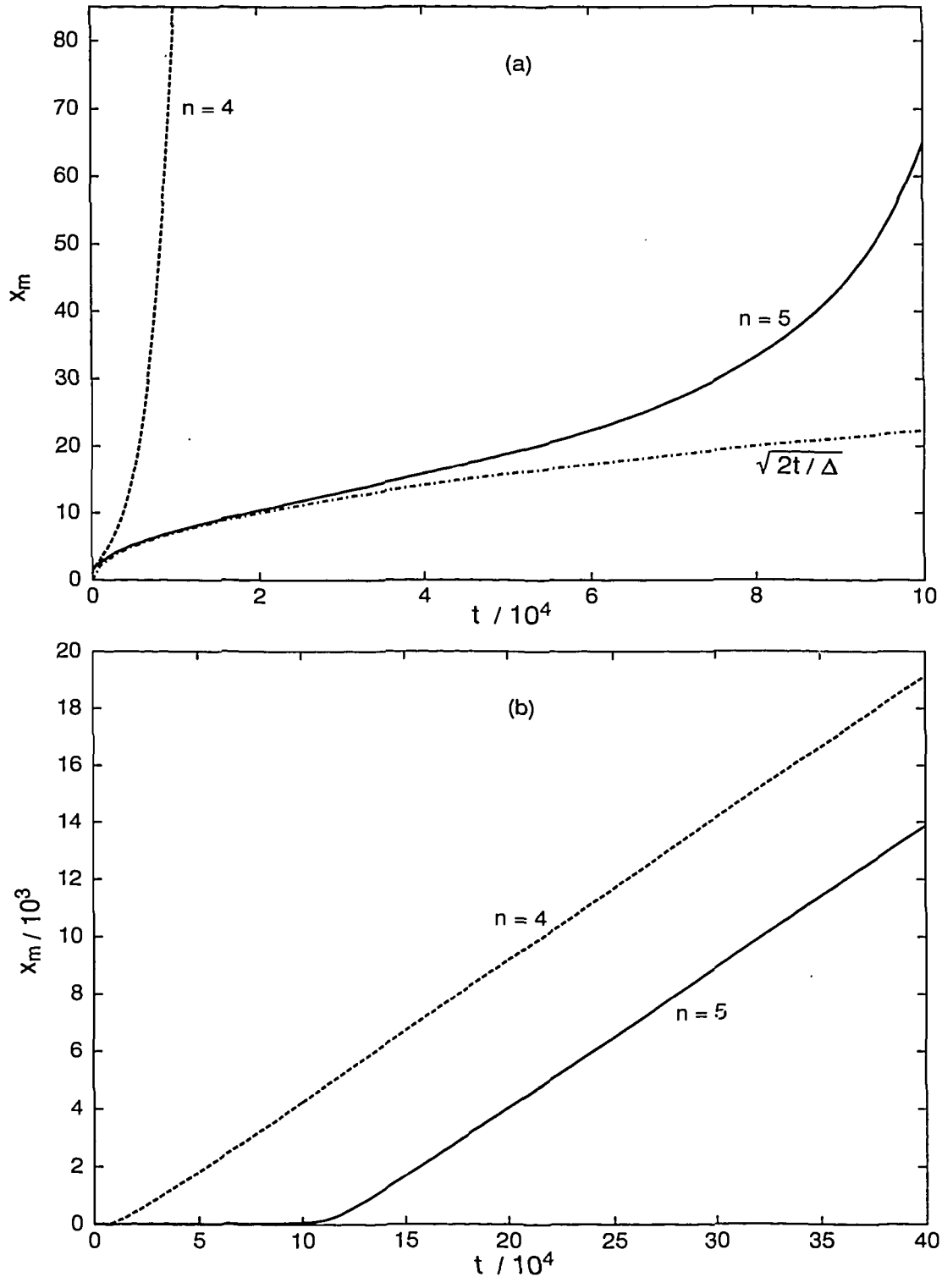

FIGURE 6: The same as Figure 5 but for $\Delta = 400$.

case (A) formulas in Equation (70) or (71). From Equation (74) we then have $t_{\rm arr}(x) = \Delta\,(x^2 - 2)/2$, and Equation (41) gives for the local degree of oxidation

$$d_o(x,t) = 1 - \exp\left(-\frac{x_m^2(t) - x^2}{2}\right). \tag{76}$$

This $d_o(x,t)$ is significantly different from 1 only for $x^2 \gtrsim x_m^2(t) - 4$. Because case (C) is in a sense intermediate between cases (A) and (B) (cf. Figure 3), it is quite possible that Equations (70) and (71) will also apply to case (C). This however still remains to be proven. Assuming that this is the case, Equation (47) would then give for the local degree of oxidation in case (C)

$$d_o(x,t) = \left(1 - \frac{x_m^2(t) - x^2}{8}\right)\frac{x_m^2(t) - x^2}{2} \quad \text{for} \quad x_m^2(t) - 4 < x^2 < x_m^2(t), \tag{77}$$

and $d_o(x,t) = 1$ for $x^2 < x_m^2(t) - 4$.

Let us mention ahead of time that for the parameters corresponding to the UO_2 fuel, the advance of the oxidation front in the case of the diffusion-controlled oxidation is also given by an equation identical with Equation (71) (cf. Equation (88) and the discussion following Equation (94)).

Garisto [3] did several calculations with a variable consumption rate corresponding to our case (B), but for a limited oxygen supply. However, his calculations may not be completely consistent because it seems that he used the formula for the degree of oxidation derived assuming that the consumption rate is constant. Here we attempt to achieve self-consistency, at least in the framework of the integral approximation and for the simpler case of unlimited oxygen supply.

3. DIFFUSION-CONTROLLED MODEL

In the limit of infinite reaction rate of oxidation, all the oxygen available at a certain position X is used up instantaneously. Oxidation is thus controlled by the rate of diffusion of oxygen through an already oxidized layer of material. In this case, the scaling constants α and β of Equations (2) and (3) go to zero, and so it is better to treat this limit separately. In this case, there is no unique scaling to dimensionless equations and thus we work in the real coordinates X and Θ. We first discuss the diffusion-controlled oxidation of a rod (defected fuel element) under unlimited oxygen supply, then briefly the same system under limited oxygen supply, and finally oxidation of a sphere under unlimited oxygen supply.

3.1 UNLIMITED OXYGEN SUPPLY IN A ROD

The geometry of the system is the same as in Section 2 – oxygen diffuses through one defected end (the cap being completely removed) of a used-fuel element. The external

oxygen concentration is constant, equal to C_0. Assume that, at time Θ, the part of the fuel element between 0 (the defect) and $X_m(\Theta)$ is completely oxidized ($d_o(X,\Theta) = 1$ for $X < X_m(\Theta)$ and $d_o(X,\Theta) = 0$ for $X > X_m(\Theta)$). The flow of oxygen through this oxidized region is governed by the simple diffusion equation

$$\frac{\partial C(X,\Theta)}{\partial \Theta} = D\,\frac{\partial^2 C(X,\Theta)}{\partial X^2}\,;\quad 0 < X < X_m(\Theta)\,. \tag{78}$$

Here D is the apparent diffusion coefficient for oxygen diffusion through the oxidized material. In principle, it can be different from D_e of Section 2. In fact, D_e may depend slightly on the degree of oxidation, which was ignored in Section 2. The solution of Equation (78) must satisfy the following evident initial and boundary conditions:

$$C(X,0) = 0\,, \tag{79}$$

$$C(0,\Theta) = C_{ex}(\Theta) = C_0\,, \tag{80}$$

$$C(X_m(\Theta),\Theta) = 0\,. \tag{81}$$

Let us now derive the condition for the velocity of the moving boundary $X < X_m(\Theta)$ between the oxidized and unoxidized regions. The total influx of oxygen into the unoxidized material at $X = X_m(\Theta)$ is given by

$$F = -\pi b^2 \varepsilon\, D \left(\frac{\partial C}{\partial X}\right)_{X=X_m}\,.$$

All this oxygen is instantaneously used in oxidation. During a time interval $d\Theta$, the total influx of oxygen (in grams) is thus

$$dW = F\,M_O\,d\Theta\,.$$

This amount is capable of oxidizing completely (from UO_2 to U_3O_7) a layer of certain thickness $dX_m(\Theta)$. The weight of unoxidized fuel contained in this layer is

$$dW_0 = \rho(1-\varepsilon)\pi b^2\,dX_m\,.$$

Complete oxidation corresponds to the weight gain of

$$\frac{dW}{dW_0} = \frac{M_O}{6\,M_f}\,.$$

Substituting here the above expressions for dW and dW_0 gives

$$\frac{dX_m(\Theta)}{d\Theta} = -R\,D \left(\frac{\partial C}{\partial X}\right)_{X=X_m}\,, \tag{82}$$

where

$$R = \frac{6\,M_f\,\varepsilon}{\rho(1-\varepsilon)} = \frac{1}{\Delta\,C_0}\,,$$

cf. Equation (13). Differentiating Equation (81) by Θ and using Equations (82) and (78) gives another condition that must be satisfied by the solution of Equation (78):

$$\left(\frac{\partial^2 C}{\partial X^2}\right)_{X=X_m} = R\left(\frac{\partial C}{\partial X}\right)^2_{X=X_m} . \tag{83}$$

Finally, by multiplying Equation (78) by X^k, $k = 0, 1, \ldots$, and integrating from 0 to $X_m(\Theta)$, one gets the following integral conditions

$$\int_0^{X_m(\Theta)} \frac{\partial C}{\partial \Theta}\, dX = D\left[\left(\frac{\partial C}{\partial X}\right)_{X=X_m(\Theta)} - \left(\frac{\partial C}{\partial X}\right)_{X=0}\right], \tag{84}$$

and

$$\int_0^{X_m(\Theta)} X^k \frac{\partial C}{\partial \Theta}\, dX = D \int_0^{X_m(\Theta)} X^k \frac{\partial^2 C}{\partial X^2}\, dX\,; \quad k = 1, 2, \ldots \tag{85}$$

In the spirit of the integral method, let us assume that

$$C(X, \Theta) = C_0 + \sum_{i=1}^{n} a_i(\Theta)\, X^i\,; \quad 0 < X < X_m(\Theta)\,, \tag{86}$$

with $X_m(0) = 0$. Substituting this into the conditions in Equations (81) through (84) and the first $n-2$ conditions in Equation (85), one can see after some manipulations that all these conditions can be satisfied for arbitrary n if

$$X_m(\Theta) = \xi\sqrt{\Theta}\,; \quad a_i(\Theta) = -\alpha_i\, \Theta^{-\frac{i}{2}}\,, \tag{87}$$

where ξ and α_i are the solution of a certain system of algebraic equations (linear in α_i and nonlinear in ξ), and they depend on n. This is true even for $n = 1$, when Equations (83) and (84) must be ignored, and when

$$X_m(\Theta) = \sqrt{2RDC_0\Theta}\,, \quad \text{i.e.,} \quad \xi^2_{n=1} = 2RDC_0 = \frac{2D}{\Delta} = \frac{12\, M_f\, \varepsilon\, C_0\, D}{\rho(1-\varepsilon)}\,, \tag{88}$$

cf. Equations (13) and (71). Substituting Equation (87) into (86) gives

$$C(X, \Theta) = C_0 - \sum_{i=1}^{n} \alpha_i \left(\frac{X}{\sqrt{\Theta}}\right)^i\,; \quad X \le \xi\sqrt{\Theta}\,. \tag{89}$$

This means that the exact solution obtained in the limit $n \to \infty$ must be of the form

$$C(X, \Theta) = \varphi\left(\frac{X}{\sqrt{\Theta}}\right), \quad X \le \xi\sqrt{\Theta} = X_m(\Theta)\,, \tag{90}$$

where $\varphi(y)$ is a function defined for $0 < y < \xi$, whose truncated Taylor series for $y = \frac{X}{\sqrt{\Theta}}$ is approximately given by Equation (89). From Equation (80) one has

$$\varphi(0) = C_0\,, \tag{91}$$

and from Equation (81),

$$\varphi(\xi) = 0\,. \tag{92}$$

Substituting Equation (90) into Equation (78) gives for $\varphi(y)$ the following ordinary differential equation:

$$\frac{d}{dy}\left(\ln\frac{d\varphi}{dy}\right) = -\frac{y}{2D}\,; \quad 0 < y < \xi\,.$$

Integrating this equation twice and using conditions Equation (91) and (92) to determine the integration constants gives

$$\varphi(y) = C_0\frac{\int_y^\xi \exp\left(-\frac{\eta^2}{4D}\right)d\eta}{\int_0^\xi \exp\left(-\frac{\eta^2}{4D}\right)d\eta} = C_0\left[1 - \frac{\operatorname{erf}\left(\frac{y}{2\sqrt{D}}\right)}{\operatorname{erf}\left(\frac{\xi}{2\sqrt{D}}\right)}\right]. \tag{93}$$

Finally, substituting Equation (90) using Equation (93) into the condition in Equation (83) or (82) gives the following relation for the value of ξ:

$$\omega\operatorname{erf}(\omega) = \frac{RC_0}{\sqrt{\pi}}e^{-\omega^2}\,; \quad \xi = 2\sqrt{D}\,\omega\,. \tag{94}$$

This equation can easily be solved numerically. Its solution is compared in Figure 7 (solid line) with the value of $\xi_{n=1}$ of Equation (88). From the form of Equation (94) it is evident that the $n = 1$ square-root dependence of ξ on D is preserved also in the exact ξ. However, the dependence of the exact ξ on RC_0 is much weaker than in the $n = 1$ approximation. Though the solid curve of Figure 7 is monotonically growing for all $\kappa = \frac{RC_0}{\sqrt{\pi}} = \frac{1}{\Delta\sqrt{\pi}}$, its derivative goes to zero as $\kappa \to \infty$ (for large κ, it approaches the inverse of $\kappa \approx \omega e^{\omega^2}$). The same solution to this problem, as given by Equations (90), (93) and (94), has been obtained using the method of matching the solutions at the moving boundary by Crank [9] when studying tarnishing reactions.

Thus the square-root dependence of the position of the oxidation front $X_m(\Theta)$ on time Θ that appeared already for $n = 1$ in Equation (88) has survived even in the exact solution. Only the exact value of ξ is given by a much more complicated implicit formula, Equation (94). However, for the UO_2 fuel, $\Delta = 15048.0$ (cf. Equation (13)), thus $\kappa = 3.75 \times 10^{-5}$. As one can see from Figure 7, for such a small value of κ, the solution of Equation (94) is identical with $\xi_{n=1}$ of Equation (88). Thus Equation (88) in this case represents very well the exact solution. Note that it has exactly the same form as Equation (71) of Section 2.4, which may be surprising at first glance because the present model differs considerably from that of Section 2.4. However, note that Equations (76) and (77) give for larger times a relatively narrow (with respect to x_m) region near x_m where the local degree of oxidation is less than 1. Only in this region can oxidation take place in the reaction-diffusion model. The same is true for case (A) of Section 2.4. Thus for larger times, there is actually not a significant difference between the two models. The main difference is at small times, represented by the difference of x_m from the parabola in Figures 5a and 5b.

This is an example where the integral method could be relatively easily carried out in all orders of n, and where it even leads to the analytical form of the exact solution.

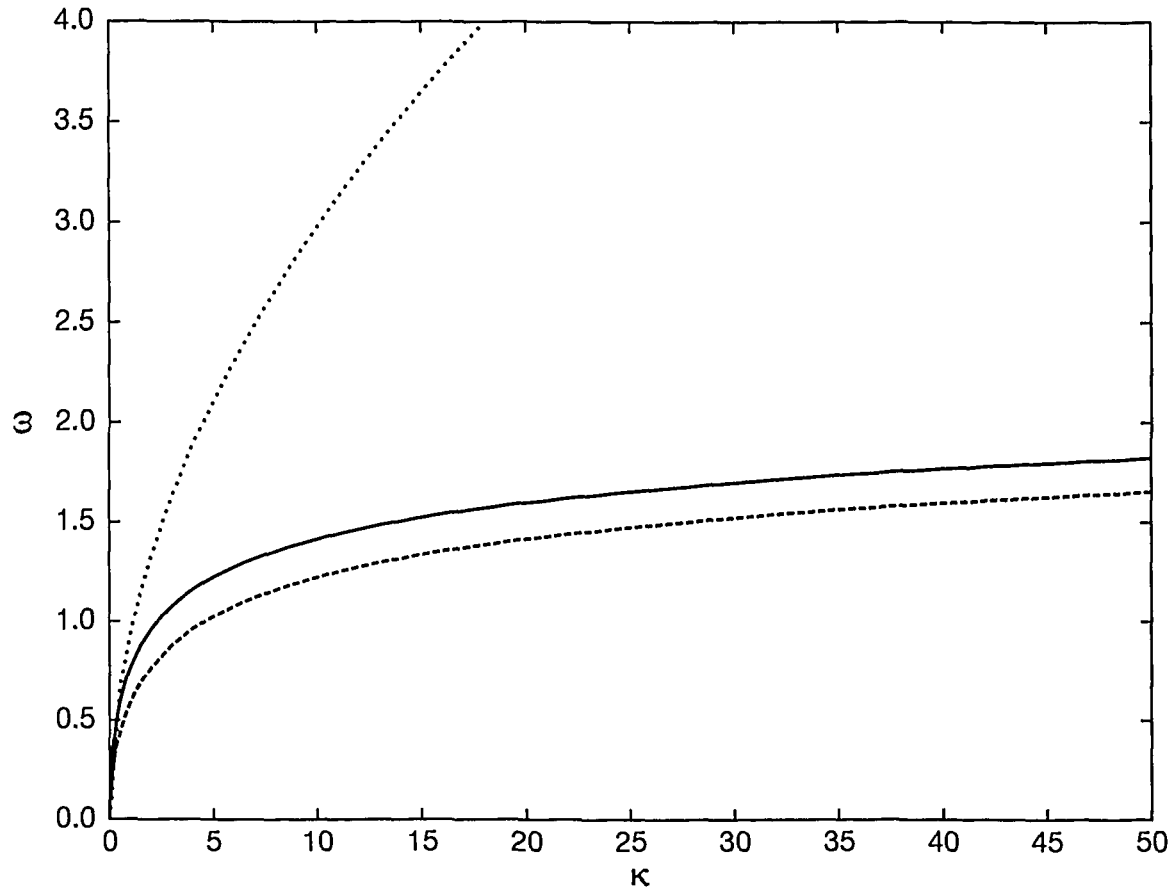

FIGURE 7: The dependence of $\omega = \frac{\xi}{2\sqrt{D}}$ on $\kappa = \frac{RC_0}{\sqrt{\pi}} = \frac{1}{\Delta\sqrt{\pi}}$. Solid line represents the solution of Equation (94) (rod) and the dashed line the solution of Equation (107) (sphere). Dotted line corresponds to the $n = 1$ formula (Equation 88), i.e, to $\omega = \sqrt{\frac{1}{2}\sqrt{\pi}\,\kappa}$.

3.2 LIMITED OXYGEN SUPPLY IN A ROD

In this case all the relations are the same as in the previous one, except that the condition in Equation (80) must be replaced by a condition of the type in Equation (26), namely

$$F_{\rm ex} = -\pi b^2 \varepsilon D \left(\frac{\partial C}{\partial X}\right)_{X=0}, \quad \frac{d}{d\Theta}(VC_{\rm ex}) = -N_d F_{\rm ex},$$

and thus

$$\frac{d}{d\Theta}C_{\rm ex}(\Theta) = Q\left(\frac{\partial C}{\partial X}\right)_{X=0}, \tag{95}$$

where $C_{\rm ex}(0) = C_0$ and

$$Q = \frac{\varepsilon N_d \pi b^2 D}{V}.$$

In this case, there seems to be no easy way to solve the integral method conditions semianalytically for arbitrary n. Ignoring the conditions in Equations (83), (84), and (85), we illustrate only the situation using $n = 1$.

Assuming that $C(X,\Theta) = a_1(\Theta)\,X + C_{ex}(\Theta)$, we get

$$C_{ex}(\Theta) = C_0 - \frac{Q}{RD}\,X_m(\Theta)\,,$$

and

$$\dot{X}_m = \frac{RDC_0}{X_m} - Q\,.$$

Integrating this gives

$$\Theta = -\frac{1}{Q}\left[X_m(\Theta) + \frac{RDC_0}{Q}\,\ln\left|1 - \frac{Q\,X_m(\Theta)}{RDC_0}\right|\right]\,. \tag{96}$$

For small Θ, $X_m(\Theta)$ must also be small. Keeping only terms up to the quadratic one in the Taylor series of the logarithm on the left-hand side of Equation (96) gives

$$x_m(\Theta) \approx \sqrt{2RDC_0\Theta}\,.$$

Thus the short time dependence of $X_m(\Theta)$ is the same as in the unlimited-oxygen-supply case (see Equation (88)), as it should be.

For $\Theta \to \infty$, $X_m(\Theta)$ is approaching the value of $\frac{RDC_0}{Q}$ from below, and the first term in the square brackets on the right-hand side of Equation (96) can be neglected; thus

$$X_m(\Theta) \approx \frac{RDC_0}{Q}\left(1 - e^{-\frac{Q^2\Theta}{RDC_0}}\right)\,,$$

and

$$C_{ex}(\Theta) \approx C_0\,e^{-\frac{Q^2\Theta}{RDC_0}}\,.$$

This exponential dependence theoretically means that infinite time is needed to consume all the available oxygen. However, the amount of remaining oxygen approaches zero very fast as time increases. Nevertheless, this behaviour is in contrast with the finite time needed to consume all oxygen in the reaction-diffusion model of Section 2.2. However, this infinite-time result in the present case still has to be confirmed by numerical calculations for higher n approximations. But in the light of the results of Section 3.1, one can expect that the $n = 1$ approximation is already a good representation of reality. Note that here when going from Section 3.1 to Section 3.2, we go from an unbounded $X_m(\Theta)$ in Section 3.1 to a bounded $X_m(\Theta)$ in Section 3.2. Thus, one can expect that the same n that already gave satisfactory results in some sense in the unbounded case, will be at least as good in the bounded case. When going from Section 2.2 to Section 2.4, the situation as regards $X_m(\Theta)$ is just the opposite – we go from a bounded case to an unbounded one, which is probably why the $n = 3$ and $n = 4$ approximations give such poor results in Section 2.4.

3.3 UNLIMITED OXYGEN SUPPLY IN A SPHERE

This particular system is used as a simple model for the oxidation of individual UO_2 grains [9-11], which is definitely a diffusion-controlled process. The grains are approximated by perfect compact spheres with no pores or cracks. Let us study the oxidation of one such sphere of radius r_0, surrounded by air with constant oxygen concentration C_0. Initially, at $\Theta = 0$, the sphere consists of UO_2 only, and the concentration of oxygen inside the sphere is equal to zero. Let us assume that at time Θ the oxidation front penetrates down to radius $r_m(\Theta)$ (measured from the centre of the sphere). The diffusion of oxygen through the oxidized layer of U_3O_7 is described by

$$\frac{\partial C(r,\Theta)}{\partial \Theta} = D\,\frac{1}{r^2}\,\frac{\partial}{\partial r}\left(r^2\,\frac{\partial C(r,\Theta)}{\partial r}\right)\;;\quad r_0 > r > r_m(\Theta)\,. \tag{97}$$

Now D is the intrinsic diffusion coefficient of oxygen in U_3O_7 (there are no pores or cracks). Substituting

$$C(r,\Theta) = \frac{1}{r}\,U(r,\Theta)$$

into Equation (97) gives an equation of the same form as Equation (78):

$$\frac{\partial U(r,\Theta)}{\partial \Theta} = D\,\frac{\partial^2 U(r,\Theta)}{\partial r^2}\;;\quad r_0 > r > r_m(\Theta)\,. \tag{98}$$

The initial and boundary conditions for U are

$$U(r,0) = 0\,;\quad 0 \le r \le r_0\,, \tag{99}$$

$$U(r_0,\Theta) = r_0\,C_0\,, \tag{100}$$

$$U(r_m(\Theta),\Theta) = 0\,. \tag{101}$$

The flux of oxygen into the unoxidized inner region of the sphere is

$$F = 4\pi r_m^2\,D\left(\frac{\partial C}{\partial r}\right)_{r=r_m}\,.$$

In the same way as in the preceding subsection, we get for the homogeneous sphere,

$$\frac{dW}{dW_0} = \frac{M_O}{6\,M_f} = \frac{F\,M_O\,d\Theta}{\rho\,4\pi r_m^2(-dr_m)}\,,$$

and thus

$$\frac{d}{d\Theta}r_m(\Theta) = -R\,D\left(\frac{\partial C}{\partial r}\right)_{r=r_m}\,, \tag{102}$$

where now

$$R = \frac{6\,M_f}{\rho}\,.$$

Because Equation (98) has the same form as Equation (78), a solution of Equation (98) satisfying conditions in Equations (*99*), (*100*), and (*101*) is

$$r\,C(r,\Theta) = u(r,\Theta) = r_0\,\varphi\left(\frac{r_0 - r}{\sqrt{\Theta}}\right)\;; \qquad r_0 > r > r_0 - \xi\sqrt{\Theta} = r_m(\Theta)\,, \tag{103}$$

where $\varphi(y)$ is again given by Equation (93).

Equation (103) gives

$$\left(\frac{\partial C}{\partial r}\right)_{r=r_m} = \frac{1}{r_m^2}\left[r_m\left(\frac{\partial U}{\partial r}\right)_{r=r_m} - U(r_m,\Theta)\right] = -\frac{r_0}{r_m\sqrt{\Theta}}\left(\frac{d\varphi(y)}{dy}\right)_{y=\xi}.$$

Substituting this expression into Equation (102) gives

$$\frac{1}{2}\frac{d}{d\Theta}r_m^2 = -\frac{RDr_0C_0}{\sqrt{\pi D\Theta}}\frac{e^{-\omega^2}}{\mathrm{erf}(\omega)}\,, \tag{104}$$

where

$$\omega = \frac{\xi}{2\sqrt{D}}\,.$$

Unfortunately, this condition cannot be satisfied identically because from Equation (103) we have

$$r_m = r_0 - \xi\sqrt{\Theta}\,. \tag{105}$$

However, one can try to satisfy Equation (104) approximately: integrating Equation (104) gives

$$r_m^2 = r_0^2 - 4RC_0r_0\sqrt{\frac{D}{\pi}}\frac{e^{-\omega^2}}{\mathrm{erf}(\omega)}\sqrt{\Theta}\,. \tag{106}$$

Let us now choose ξ so that at least the duration of the complete oxidation of the whole sphere is the same as given by Equations (105) and (106). The oxidation stops when the oxidation front reaches the centre of the sphere, that is, when $r_m = 0$ (remember, here we are studying the oxidation to U_3O_7 only; at higher temperatures, the oxidation to U_3O_8 continues even after that). Let this happen at time Θ_{end}. Then requiring that $r_m = 0$ corresponds to the same Θ_{end} in both Equations (105) and (106), we have

$$\Theta_{\mathrm{end}} = \left(\frac{r_0}{\xi}\right)^2,$$

and

$$\omega\,\mathrm{erf}(\omega) = 2\kappa e^{-\omega^2}\;; \quad \xi = 2\sqrt{D}\,\omega\;; \quad \kappa = \frac{RC_0}{\sqrt{\pi}}\,, \tag{107}$$

which is almost the same as the condition in Equation (94) except for the additional factor of 2. Because of this factor, $\omega_{\mathrm{sphere}}(\kappa) = \omega_{\mathrm{rod}}(2\kappa)$. The solution of Equation (107) ($\omega_{\mathrm{sphere}}(\kappa)$) is represented in Figure 7 by the dashed line. One can see that for the

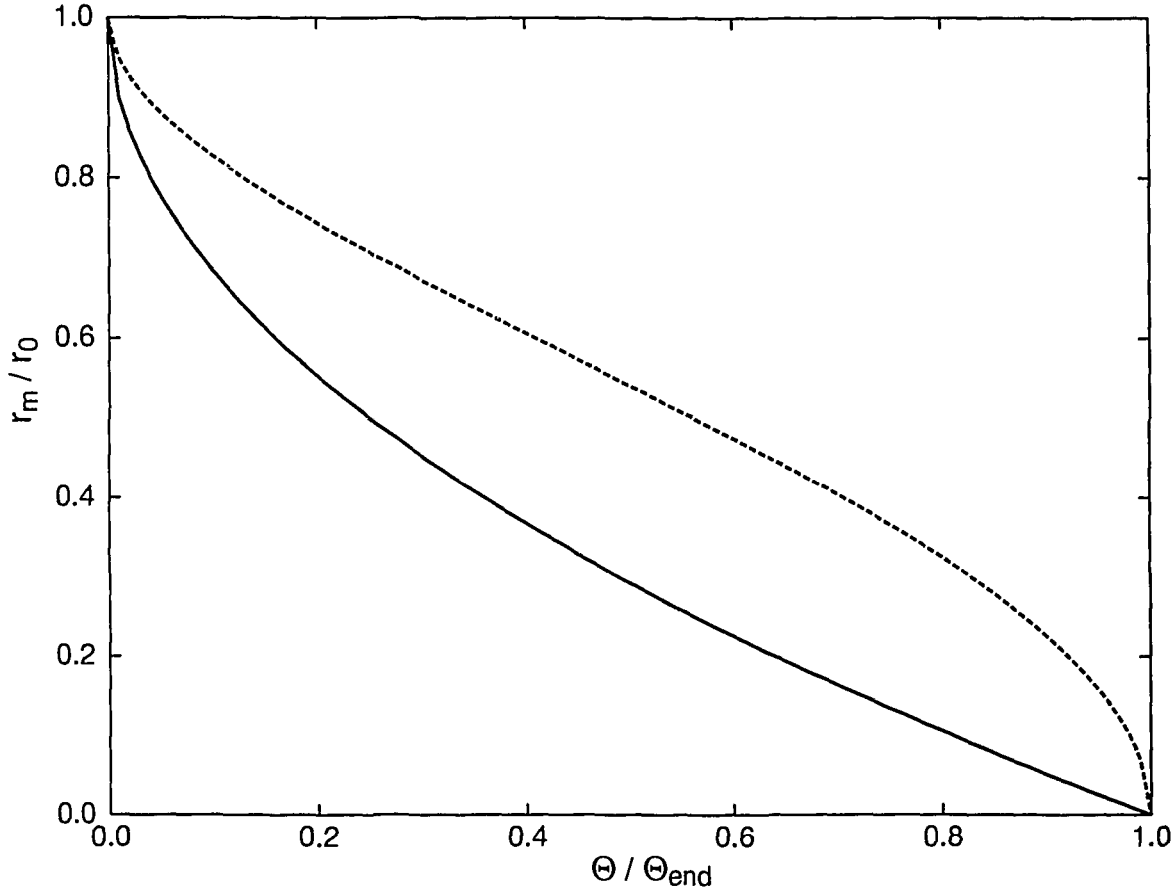

FIGURE 8: Comparison of Equations (108) (solid line) and (109) (dashed line). r_0 is the radius of the sphere, r_m is the position of the oxidation front at time Θ, and $\Theta_{end} = (r_0/\xi)^2$ is the time necessary for the complete oxidation of the whole sphere to U_3O_7.

exactly identical parameters, the (approximate) speed of the oxidation front in a sphere is smaller than that in the rod.

Equation (105) can be written as

$$\frac{r_m}{r_0} = 1 - \sqrt{\frac{\Theta}{\Theta_{end}}}, \tag{108}$$

and, using ξ determined by Equation (107), Equation (106) becomes

$$\frac{r_m}{r_0} = \sqrt{1 - \sqrt{\frac{\Theta}{\Theta_{end}}}}. \tag{109}$$

These two expressions are compared in Figure 8. Their difference represents the degree of approximation with which Equations (103) and (107) solve the spherical problem.

Hopefully, the application of the higher n integral approximations directly to the spherical problem would lead to the exact form of $r_m(\Theta)$, although it may not be

possible to write it in a simple analytical form. Here let us just note that the linear $n = 1$ approximation gives exactly the same expression for ξ as in the case of a rod. A first degree polynomial satisfying Equations (100) and (101) has the form

$$C(r, \Theta) = C_0 \frac{r - r_m}{r_0 - r_m} .$$

This linear expression is the steady state of Equation (97). Thus the $n = 1$ approximation corresponds in this case to the quasi-steady-state approximation. This gives

$$\frac{\partial C}{\partial r} = \frac{C_0}{r_0 - r_m} ,$$

and then from Equation (102),

$$r_0 - r_m = \sqrt{2RDC_0\Theta} . \tag{110}$$

This is exactly the same dependence as in Equation (88). Thus the dotted curve of Figure 7 applies to both cases. Equation (110) is often used for the analysis of the experiments studying the oxidation of UO_2 powders [9-11], However, as we have discussed above, its square-root dependence on $D\Theta$ seems to be only an approximation.

The relative weight gain (r.w.g.) of the whole sphere is evidently equal to

$$\text{r.w.g.} = \frac{M_O}{6M_f} \left[1 - \left(\frac{r_m}{r_0} \right)^3 \right] . \tag{111}$$

In Figure 9 we compare the time dependence of this weight gain corresponding to the two approximate formulas in Equations (108) and (109). The shapes of the two curves agree well with experimental data, for example as presented in Figure 1 of Ref. [14], Figures 4 and 7 of Ref. [21], Figure 1 of Ref. [18], or Figure 2 of Ref. [16]. The main difference is that the initial slope of most experimental curves is finite (an exception being Figure 1 of Ref. [14] where the initial slope seems to be infinite), whereas the initial slope of the two curves in Figure 9 is infinite, as can be seen easily by differentiating Equation (111) by Θ. It is the initial slope of the experimental curves for the irradiated CANDU fuel as measured by Hastings et al. [15] (see also Ref. [19] - CANDU fuel seems to give clearly an initial linear dependence of weight increase on time) that was used to calculate the rate K_{v0} of oxygen consumption in Ref. [3] (see Equation (114) in what follows).

We have also calculated the time dependence of the relative weight gain for an ensemble of spheres with uniformly distributed radii in a certain interval for Equation (108). The form of this dependence is practically the same as the one for a single sphere (solid line in Figure 9), also having an initial infinite slope. The only difference is that for the same Θ, r.w.g. slightly increases with the spread in radii.

Actually, most of the previous authors† did not attempt to derive the dependence of ξ on D and C_0. They usually assumed that Equation (105) holds with $\xi = r_0 \sqrt{k'}$, where

†An exception is Equation (4) of Ref. [13] or Equation (2) of Ref. [10] that contains the expression $2RDC_0\Theta$ and is a variation of Equation (111) using (110) ($n = 1$), and gives curves similar to the ones in Figure 9.

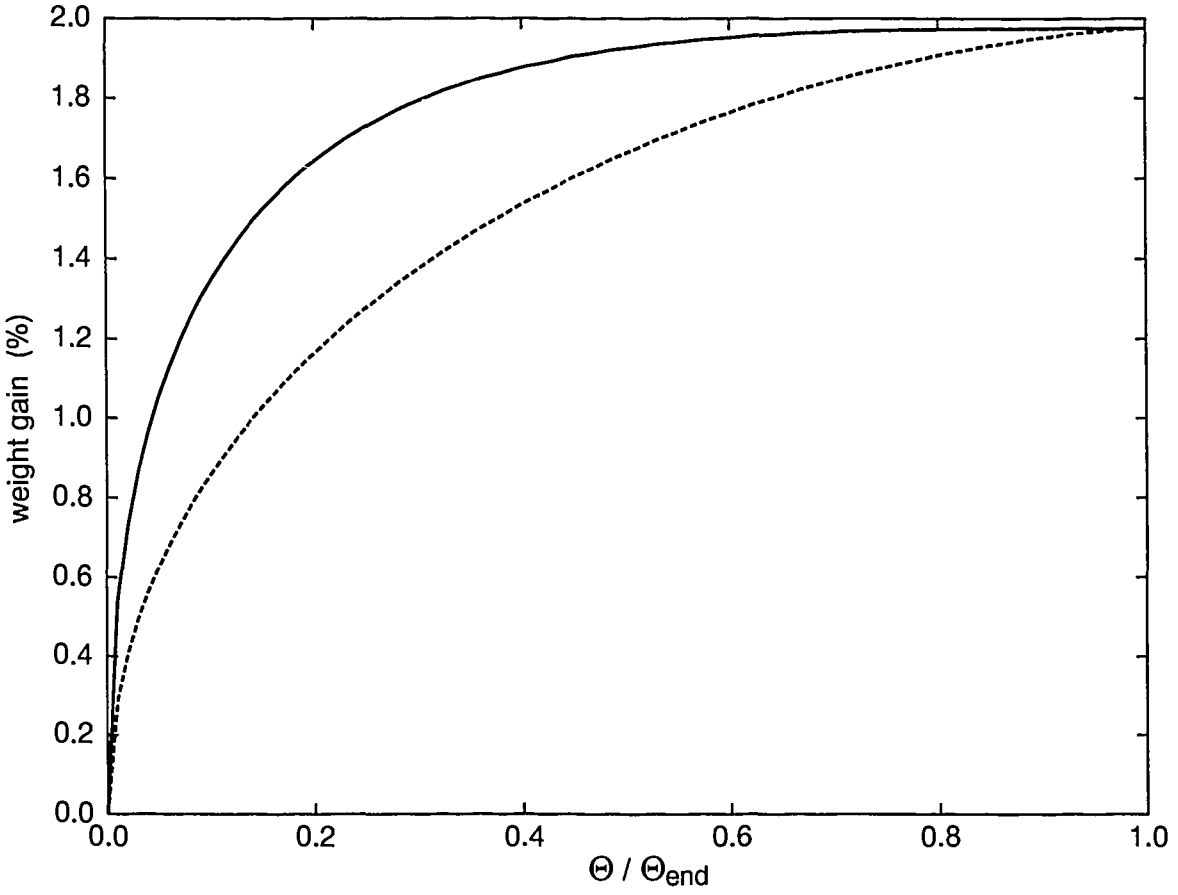

FIGURE 9: Comparison of the time dependence of the relative weight gain of the whole sphere corresponding to Equations (108) (solid line) and (109) (dashed line).

k' is called a "rate constant" (see e.g. Equation (9) of Ref. [11]) or "oxidation rate constant" [12], and is calculated from experimental data. In the notation introduced above, $k' = \Theta_{end}^{-1}$. Note that the experimental data in Figure 7 of Ref. [11] (see also Figure 7 in [12]) correspond more closely to Equation (108) than (109), except for small times where the oxidation rate is much smaller than as given by Equation (108). This was attributed in [11] to the so-called oxidation incubation, but it may also at least partially correspond to the initial portion of the dashed curve in Figure 8.

The k' values, as calculated from experimental data by Woodley et al. [12], depend to some extent on the degree of oxidation, which confirms the fact that Equation (108) holds only approximately in the spherical case.

The weak dependence of ξ on C_0 in Equation (107) (Figure 7) justifies the choice of the oxygen-consumption term in Equation (1) as being independent of C.

3.4 A MODIFIED REACTION-DIFFUSION MODEL

Now that we have found in Section 3.3 the dependence of ξ on the concentration of oxygen at the external surface of a spherical grain, one can, at least in principle, use the results of the previous subsection to derive a more realistic dependence on time (degree of oxidation) of the consumption rate K_v used in the equivalent porous medium model of Section 2. Let us assume again that we have a system of cracks and pores described by porosity ε and an apparent diffusion constant D_e, and that the individual grains can be approximated by spheres of radius r_0, and the oxidation of the grains proceeds as described in Section 3.3. Then the rate of consumption of oxygen at a position X may be derived from Equation (111) using r_m/r_0 given by Equation (108) with Θ substituted by $\Theta - \Theta_{\rm arr}$ and ξ given by Equation (107) where C_0 is substituted by $C(X,\Theta)$:

$$\varepsilon K_v = \frac{1-\varepsilon}{M_O V_0}\frac{d}{d\Theta}[V_0 \rho \text{ r.w.g.}] = \frac{1-\varepsilon}{R}\frac{d}{d\Theta}\left[1-\left(\frac{r_m}{r_0}\right)^3\right] . \qquad (112)$$

Here $V_0 = \frac{4}{3}\pi r_0^3$ is the volume of the idealized spherical grain. This will represent a good approximation only if $C(X,\Theta)$ will change slowly at the position X over the time interval $\Theta_{\rm arr} \le \Theta \le \Theta_{\rm arr} + \Theta_{\rm end}$ because the formulas of Section 3.3 were derived assuming that C_0 is constant. However, in view of the weak dependence of ξ on C_0 through the formula in Equation (107), it is possible that moderate variation of $C(X,\Theta)$ will not pose substantial problems. In this way, the "order of reaction" would be automatically taken care of. In any case, the practical application of Equation (112) will require further studies.

4. COMPARISON WITH THE CEX-1 EXPERIMENT

It was observed during the first (after 41 months in dry air at 150°C) and second (after another 58.5 months) examinations that different bundles had oxidized at rather different rates. Thus the consumption of oxygen was not distributed equally among all defected elements (there were 56 defected elements in the first storage period, and 52 in the second one – four elements were removed for destructive examination during the first interim examination). Bundle FO6605C was selected for more detailed second examination because it experienced the greatest amount of UO_2 oxidation during the first 41 months of the experiment, much larger than other bundles. Thus most of the oxygen available for fuel oxidation was probably consumed by its 15 defected elements. In Ref. [3] it was assumed that all defected elements were exactly identical, and $N_d = 52$ was used.

Element 8 of bundle FO6605C used in Ref. [3] for the comparison with limited-supply model calculations actually underwent two oxidation cycles. There is no doubt that during the first storage period (41 months) the oxygen supply was really limited – the extent of oxidation found at the first examination was even lower than expected with 56 defected elements. It is likely that a part of the available oxygen was consumed by the

oxidation of other (steel) components of the CEX-1 pressure vessel and the containers in which the fuel bundles were stored. Unfortunately, no analysis of the composition of the atmosphere remaining in the pressure vessel was performed at the first examination.

During the second examination a leak was detected in the defected bundle compartment. However, it was impossible to determine when this leak actually started, whether it existed for some time before the second examination, or whether it appeared only during the opening of the CEX-1 pressure vessel at the time of the second examination.

These facts show that neither of the two limited-air-supply CEX-1 storage periods provide an ideal test case for the theoretical calculations of Ref. [3], or of this report. The degree of oxidation experienced by the CEX-1 fuel elements during the two storage periods differed considerably. The degree of oxidation of different fuel bundles in the same storage period also varied considerably. In this situation, it is perhaps possible to apply the theory of Section 2.3 at least to the elements that experienced the largest oxidation, those from bundle FO6605C, which evidently must have controlled the time dependence of $C_{ex}(\Theta)$. Then N_d to be used in formulas of Section 2.3 cannot be the actual total number of defected elements stored with air volume V, but an effective number such that V/N_d represents the volume of air consumed by the oxidation of one FO6605C defected element. One can estimate the effective value of N_d from the appearance of the sections of destructively examined elements during the first and second interim CEX-1 examinations.

The following numerical values corresponding to the CEX-1 experiment are well defined:

$$\begin{aligned} &V = 4.21 \times 10^4 \text{ cm}^3, && C_0 = 8.55 \times 10^{-6} \text{ mol} \cdot \text{cm}^{-3}, \\ &b = 0.6 \text{ cm}, && \rho = 10.97 \text{ g} \cdot \text{cm}^{-3}, \\ &\varepsilon = 0.05, && M_f = 270 \text{ g} \cdot \text{mol}^{-1}. \end{aligned} \tag{113}$$

Oxygen contained in the above volume V can oxidize completely to U_3O_7 the length, $\frac{6 M_f V C_0}{\rho (1-\varepsilon) \pi b^2} = 49.5$ cm, of a UO_2 fuel element of radius b and total porosity ε. The sum of all the oxidized islands of element 3 of bundle FO6605C (examined destructively after the first CEX-1 storage period of 41 months) seems to correspond to complete oxidation of at most 1 to 2 mm of the length of the element. All the oxidation appears to occur within 1 cm on both sides of the defect. No traces of U_3O_7 were found by chemical analysis beyond this distance from the defect. Because in our calculations we have assumed a one-sided diffusion from the defect, a real element defected somewhere along its length roughly corresponds to two idealized geometries studied in the previous sections. Thus the total amount of the oxidized material in one idealized element would correspond to N_d between 49.5/0.1 and 49.5/0.05, that is, to $N_d = 495$ to 990. This is a much larger number than the actual total number of defected fuel elements, 56, indicating that most of the oxygen trapped in the CEX-1 vessel was consumed by oxidation of something other than the fuel elements. This casts doubt on our assumption that FO6605C elements controlled fully the time dependence of $C_{ex}(\Theta)$ during the first storage period.

During the second examination (after the second storage period of 58.5 months), the amount of oxidation found in the vicinity of the defect of element 8 of bundle FO6605C was much higher - corresponding to about 4 to 5 cm of completely oxidized element, and the oxidation was confined within about 5 cm on both sides of the defect [2]. This would correspond to $N_d = 19.5$ to 24.4. This is much less than the actual total number of defected fuel elements, 52, but it is only slightly higher than the number of defected elements in bundle FO6605C, which is 14. Because other bundles apparently experienced much less oxidation, this would indicate that during the second storage period the oxidation of other components of the pressure vessel was insignificant, and that the reported leak probably really occurred only during the second examination (otherwise the extent of oxidation would be much larger).

The basis of comparison of the CEX-1 limited-air data with the equivalent medium model are Equations (32), (33), and (34), provided the value of P of Equation (27) is small enough.

In addition to the values in Equation (113), Garisto [3] used the values

$$K_{v0} = 4.12 \times 10^{-10} \text{ mol} \cdot \text{cm}^{-3} \cdot \text{s}^{-1} ,$$

and

$$D_e = 0.1905 \text{ cm}^2 \cdot \text{s}^{-1} .$$

Substituting these values into Equation (33) gives $X_{\max} = 89.5$ cm. This is much larger than what was found in the CEX-1 examinations, which is the essence of the discrepancy reported in Ref. [3]. Let us now investigate whether these values can be modified somewhat to get a better agreement with the CEX-1 results. The above value of D_e is more or less a plausible guess [3]; we do not know about any experiments directly measuring this quantity. On the other hand, the value of K_{v0} is based on apparently reliable experiments. It was derived in Ref. [3] using the formula

$$K_{v0} = F \frac{\rho(1-\varepsilon)}{3600 \times 100\, \varepsilon\, M_O} ,$$

where

$$F = 1.53 \times 10^{10} \exp\left(-\frac{(120 \pm 10) \times 10^3 \text{ J} \cdot \text{mol}^{-1}}{R_g T} \right) \tag{114}$$

is the weight increase rate in $\%\cdot h^{-1}$, $R_g = 8.3144$ J (mol·K)$^{-1}$, and T is absolute temperature. Formula (114) was obtained from oxidation experiments conducted at 175 to 400°C on small fragments of irradiated CANDU fuel [15]. It gives values that are of the same order as the weight increase rates for other types of fuel (cf. Figure 1 of Ref. [16] or Figure 4 of Ref. [21]). However, extrapolating this formula to the temperature of 150°C may give values that are too small. In Table 1, we compare the values given by Equation (114) with the values of the average rate of weight increase calculated from Table III of Ref. [12] for powders and fragments of irradiated pressurized-water reactor (PWR) fuel with linear heat rating much smaller than that of CANDU fuel. These

average rates of weight increase were obtained simply by dividing the total weight increases of Table III of Ref. [12] by the respective duration of oxidation. Data obtained in the $^{18}O_2$ atmosphere were rescaled to normal air. One can see that the values of F obtained in this way from Ref. [12] are, especially for lower temperatures, up to one order of magnitude higher than those given by Equation (114). Although PWR fuel has a lower linear heat rating, it also has smaller grain size, higher porosity and higher burnup than CANDU fuel. The net effect is to make PWR fuel more reactive for the UO_2 to U_3O_7 step of oxidation. Thus the higher consumption rate obtained from the results of Woodley is not conclusive enough by itself. However it is fully in agreement with the average value of the activation energy for the UO_2 to U_3O_7 oxidation equal to 108 kJ·mol^{-1} obtained by averaging all the published values [22]. Substituting this smaller value of the activation energy into Equation (114) gives

$$K_{v0} = 1.3 \times 10^{-8}\ \mathrm{mol \cdot cm^{-3} \cdot s^{-1}}.$$

TABLE 1.

COMPARISON OF WEIGHT INCREASE RATES

Temperature (°C)	F from Equation (114)	F from Woodley et al. [12]
140.0	1.03×10^{-5}	1.57×10^{-4}
154.9	3.49×10^{-5}	9.66×10^{-5}, 2.04×10^{-4}
155.4	3.62×10^{-5}	1.25×10^{-4}
175.2	1.60×10^{-4}	1.07×10^{-3}
175.6	1.65×10^{-4}	3.83×10^{-4}
200.2	8.76×10^{-4}	1.87×10^{-3}
200.4	8.88×10^{-4}	1.60×10^{-3}
224.0	3.77×10^{-3}	5.15×10^{-3}
224.9	3.98×10^{-3}	4.63×10^{-3}
225.0	4.00×10^{-3}	4.83×10^{-3}
225.2	4.05×10^{-3}	4.16×10^{-3}

This higher value of K_{v0} is consistent with the fact that the activation energy of 120 kJ·mol^{-1} occurring in the formula in Equation (114) is actually a "mixed" activation energy corresponding to simultaneous oxidation to U_3O_7 and U_3O_8 at higher temperatures. In addition to this high value of K_{v0}, for the comparison with the CEX-1 limited-air data we also use the value

$$K_{v0} = 4.0 \times 10^{-9}\ \mathrm{mol \cdot cm^{-3} \cdot s^{-1}},$$

which roughly corresponds to Woodley's results in Table 1, and is only one order of magnitude larger than the value used by Garisto.

Note that Woodley et al. [12] did not interpret their data in terms of F (the initial portions of most of their weight-increase curves were not very linear) but in terms of

the rate k' discussed at the end of Section 3.3. How to best interpret this kind of data seems to be an open question. The real significance of K_{v0} is not very clear in the light of the discrepancy between theoretical infinite initial slopes and experimental finite ones. Also, K_{v0} can contain some effect of the diffusion through the pores of the experimentally studied fragments that hardly ever consist of single grains, i.e., a portion of what should actually be completely described by D_e. However, without further work on Equation (112) we are not yet ready to use the values of k'.

Let us now return to the comparison of Equations (32), (33), and (34) with the CEX-1 limited-air data. Note that $X_{\max}$ of Equation (33) does not depend at all on the total amount of air, V/N_d, used up in a single element. Thus $X_{\max}$ attained during the first and second storage periods should be the same (because the maximum local degree of oxidation assuming $X_{\max} = 1$ cm in the first storage period does not exceed 20%, under the assumptions of Section 2.3, the oxidation experienced in the second cycle would just be superimposed on that of the first cycle – i.e., would take place in the same spatial region around the defect). Thus, assuming that Equation (1) with the somewhat controversial K_{v0} is relevant to the CEX-1 experiment, there are at least three different possible scenarios for the first and second storage periods, as outlined below.

(i) $X_{\max} = 1$ cm in the first storage period and $X_{\max} = 5$ cm in the second period. Then assuming that C_0 is the same in both storage periods, the second period cannot correspond to a limited-air-supply situation, and the leak would have occurred sometime during the second period, leading probably to a situation of unlimited oxygen supply at substantially decreased oxygen concentration (assuming that the leak was a very small one). To obtain $X_{\max} = 1$ cm from Equation (33) would require the values given in Table 2 for the maximum degree of oxidation (Equation 32) and the total duration of the process (Equation 34). Here 1 average month = 30.4375 d. The value of P in all cases is well below 0.1 (below 0.01 for the larger values of K_{v0}), thus the QSSA approximation is well justified. These values of D_e seem to be unrealistically low. Thus the scenario (ii) described below is more probable.

TABLE 2.

PARAMETER VALUES FOR SCENARIO (i)

K_{v0} (mol · cm^{-3} · s^{-1})	D_e (cm^2 · s^{-1})	N_d	$d_o(0,\infty)$	$\Theta_{\text{dep}}(0)$ (months)
4.0×10^{-10}	0.000023	495	0.2	24.45
		990	0.1	12.22
4.0×10^{-9}	0.000234	495	0.2	2.44
		990	0.1	1.22
1.3×10^{-8}	0.000760	495	0.2	22.90 days
		990	0.1	11.45 days

(ii) $X_{\max} = 5$ cm in both the first and second storage periods. Namely, the amount of oxidation in the first period was so low that it is almost impossible to try to estimate

visually for this case the spatial dependence of the local degree of oxidation, because the extent of the oxidized areas is smaller than the irregularities of the network of cracks and pores. Thus it is plausible that under some suitable averaging, $X_{max} = 5$ cm also in the first period. Then one can satisfy Equations (32), (33), and (34) with the parameter values given in Table 3. Again, the value of P in all the above cases is well below 0.1 (below 0.01 for the larger values of K_{v0}). Here the values of K_{v0} between 4.0×10^{-9} and 1.3×10^{-8} mol $\cdot$ cm$^{-3} \cdot$ s^{-1}, and D_e between 0.005848 and 0.019 cm$^2 \cdot$ s^{-1} might correspond to reality. $D_e = D/\tau^2$, where the diffusivity of oxygen in air is $D = 0.381$ cm$^2 \cdot$ s^{-1}. This would give tortuosity between $\tau = 4.5$ and 8, which may be too high. The oxidation in the second period takes place for a significant fraction of the duration of the storage, i.e., it is much slower than predicted in Ref. [3]. The relatively short times for $\Theta_{dep}(0)$ in the first storage period reflect the fact that only a very small portion of the available oxygen is used up by the fuel elements. In any case, the data for the first storage period should not be given too much significance in the comparison of our theory with the CEX-1 results. It is quite possible that rapid, shallow oxidation of all exposed UO_2 surfaces occurs before any observable thickening of the U_3O_7 layer takes place. Such an incubation period is not described by the present theory. It would provide another fast oxygen sink during the first storage period in addition to the oxidation of the carbon-steel components of the experimental setup.

TABLE 3.

PARAMETER VALUES FOR SCENARIO (ii)

K_{v0} (mol $\cdot$ cm$^{-3} \cdot$ s^{-1})	D_e (cm$^2 \cdot$ s^{-1})	Storage Period	N_d	$d_o(0,\infty)$	$\Theta_{dep}(0)$ (months)
4.0×10^{-10}	0.000594	1	495	0.04	4.89
			990	0.02	2.44
		2	20	0.99	121.02
			25	0.79	96.82
4.0×10^{-9}	0.005848	1	495	0.04	14.88 days
			990	0.02	7.44 days
		2	20	0.99	12.10
			25	0.79	9.68
1.3×10^{-8}	0.019	1	495	0.04	4.58 days
			990	0.02	2.29 days
		2	20	0.99	3.72
			25	0.79	2.97

(iii) The third plausible scenario is that the oxidation of defected fuel elements was in the first storage period so much slower than the oxidation of other components of the experimental setup that a rapid decrease of the oxygen concentration in the pressure vessel to about 1/25 of the original concentration occurred. This reduced concentration then played the role of the modified C_0 for the fuel oxidation. This led to $X_{max} = 1$ cm and to the effective N_d decreased by a factor of 25. This in turn increased the values of

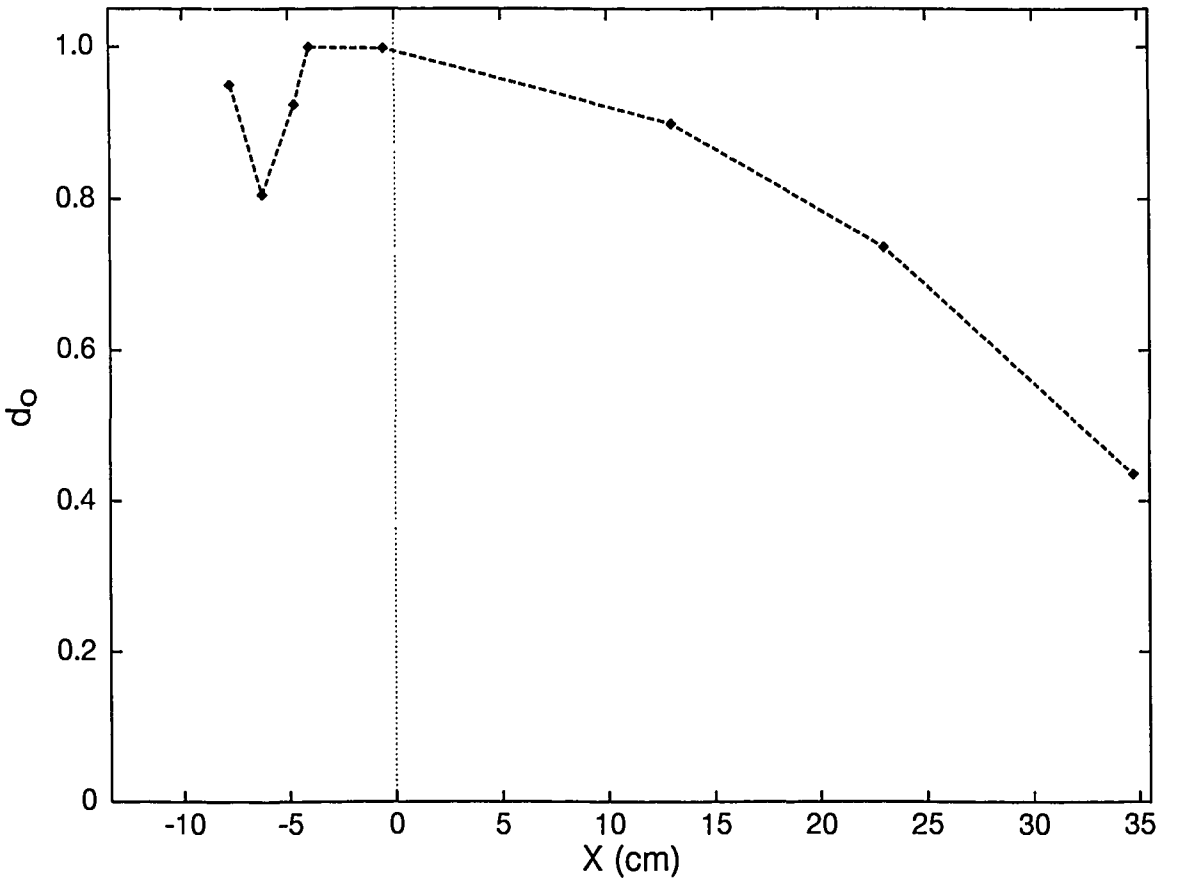

FIGURE 10: Spatial dependence of the local degree of oxidation in element 14 of bundle FO6605C after 40 months of storage in unlimited air supply. The defect position is taken as the coordinate origin $X = 0$. Data points (connected by a dashed line for convenience) were obtained from the photomacrographs of several longitudinal and transverse sections of the fuel element, and represent the fraction of the area of a given section that experienced grain pullout due to oxidation. All sections except those corresponding to the the fourth and sixth data points were longitudinal, 1.5 to 3 cm long. For these sections, the positions of data points correspond to their centres. Near the left end of the element, d_o could not be determined in this way because fuel grains fell out when cutting the element.

$d_o(0,\infty)$ and $\Theta_{dep}(0)$ by a factor of 5, giving the total duration of oxidation in the range from 1.22 to 2.44 months for $K_{v0} = 4.0 \times 10^{-9}$ mol $\cdot$ cm$^{-3} \cdot$ s^{-1}. All the values for the second period would be the same as in the preceding case (see Table 3) because the oxidation of other parts does not seem to play any significant role in the second period. Thus assuming different effective values of C_0 in the two storage periods could lead to different values of X_{max} in accordance with Equation (33).

Because the oxidized areas were relatively small, the results of the first and second CEX-1 examinations could perhaps also be interpreted as corresponding to diffusion-controlled oxidation characterized by a sharp transition in the degree of oxidation between 1 and 0 at some distance from the defect (see Section 3.2). That was one of the reasons why the diffusion-controlled oxidation was studied in Section 3. One could imagine that the pores are originally practically closed ($D_e \to 0$), and they open only as the result of the slight volume shrinkage as UO_2 is oxidized to U_3O_7, thus allowing a significant diffusion of oxygen only after the passage of the oxidation front. There is good experimental evidence that the passage of the oxidation front really opens up the grain boundaries in the unirradiated UO_2 and probably also in irradiated CANDU fuel [23].

However, planimetric data (see Figure 10) from the third CEX-1 interim examination performed after the third storage period of 40 months with unlimited air supply of dry air at 150°C (preceded by 41 + 58.5 months under limited-air-supply conditions) are not particularly compatible with a diffusion-controlled process on the scale of the whole fuel element. Nevertheless, the actual oxidation of individual fuel grains is almost certainly a diffusion-controlled process. Preliminary results of Section 3.2 suggest that in such a process with limited air supply, all oxygen can never be consumed in a finite time. Thus the small amount of oxygen found in the remaining atmosphere in the defected bundle compartment of the CEX-1 pressure vessel at the time of the second examination might be the signature (at least if we could be sure that it was not caused by the leak discussed above) of the diffusion-controlled oxidation of individual grains that cannot at present be taken into account by an equation of type (1), but could hopefully be considered in the future by an equation of type (112).

In the end, let us attempt to compare the unlimited-air data of Figure 10 with our results of Section 2.4. The comparison is somewhat complicated by the fact that (i) in the homogeneous equivalent porous medium model, d_o decreases at any given instant monotonically with the distance from the defect, whereas in a real fuel element the random network of cracks and grain boundaries can result in a nonmonotone spatial dependence of d_o; (ii) most points in Figure 10 were obtained from longitudinal sections of the fuel element that sample only a tiny part (a straight line) of the transverse cross-section at a given value of X, which might also contribute to the nonmonotone behaviour of d_o to the left of the defect in Figure 10; (iii) a real fuel element has a finite length and a defect in its circumferential cladding, whereas our simple theory is formulated for the semi-infinite case with the defect in the end cap.

The subjects of our comparison are essentially Equations (75), (72), (76) and (77). Since the duration of oxidation is 40 months, let us introduce the abbreviations

$X_{40} = X_m(\Theta = 40\,\text{months})$ for the position of the oxidation front after 40 months, and $N_{40} = \frac{40\,\text{months}}{\beta\Delta}$ for the number of plateaus of Figure 4 corresponding to the duration of the third storage period. In case (A), $X_{40} = X_{\max}\sqrt{[N_{40}]+1}$. The experimental value from Figure 10 is $X_{40} \gtrsim 36\,\text{cm}$.

For the parameter values that gave $X_{\max} = 5\,\text{cm}$ in the limited-air-supply case, we obtain from Equations (75) and (72) the values in Table 4. All three parameter sets give an X_{40} that is much smaller than the experimental value of Figure 10. The largest value of X_{40} gives the last parameter set, but even this set gives a very poor agreement with the third-examination data, as shown in Figure 11a. The rest of Figure 11 shows plots of $d_o(X, 40\,\text{months})$ corresponding to parameters modified in various ways to get a better agreement with the CEX-1 data of Figure 10.

TABLE 4.

VALUES CHARACTERIZING THE THIRD, UNLIMITED-AIR, STORAGE PERIOD OF THE CEX-1 EXPERIMENT FOR THE PARAMETERS OF TABLE 3

K_{v0} ($\text{mol}\cdot\text{cm}^{-3}\cdot\text{s}^{-1}$)	D_e ($\text{cm}^2\cdot\text{s}^{-1}$)	$\beta\Delta$ (months)	X_{40} (cm)		N_{40}
			case (A)	case (B)	
4.0×10^{-10}	0.000594	122.3	5.0	5.76	0.327
4.0×10^{-9}	0.005848	12.23	10.0	10.33	3.27
1.3×10^{-8}	0.019	3.76	16.58	17.05	10.63

Assuming that there is increased oxidation near the ends of the fuel element in comparison with d_o of a semi-infinite rod, Figure 10 could in a semi-infinite rod correspond to X_{40} as high as 46 cm. Requiring that $X_{40} = 46$ cm and that $d_o(X, 40\,\text{months}) < 1$ for $X > 10$ cm gives the situation shown in Figure 11b. Because the theoretical d_o profiles decrease rather sharply near X_m, the agreement between experimental and theoretical curves in Figure 11b is still rather poor. It gets much better when one requires $X_{40} = 37$ to 38 cm as shown in Figures 11c,d,e.

All the parameter sets used in Figure 11 are summarized in Table 5.

TABLE 5.

PARAMETER SETS USED IN FIGURE 11

Figure 11	K_{v0} ($\text{mol}\cdot\text{cm}^{-3}\cdot\text{s}^{-1}$)	D_e ($\text{cm}^2\cdot\text{s}^{-1}$)	$\beta\Delta$ (months)	X_{40} (cm)		N_{40}	$X_{\max}$ (cm)
				case (A)	case (B)		
a	1.3×10^{-8}	0.0190	3.76	16.58	17.05	10.63	5
b	2.5675×10^{-9}	0.1513	19.05	45.26	46.0	2.10	26.13
c	2.6390×10^{-9}	0.0979	18.54	36.06	37.0	2.16	20.82
d	3.0×10^{-9}	0.0734	16.31	35.42	38.0	2.45	20.45
e	2.0×10^{-9}	0.0608	24.46	32.23	37.0	1.64	22.79

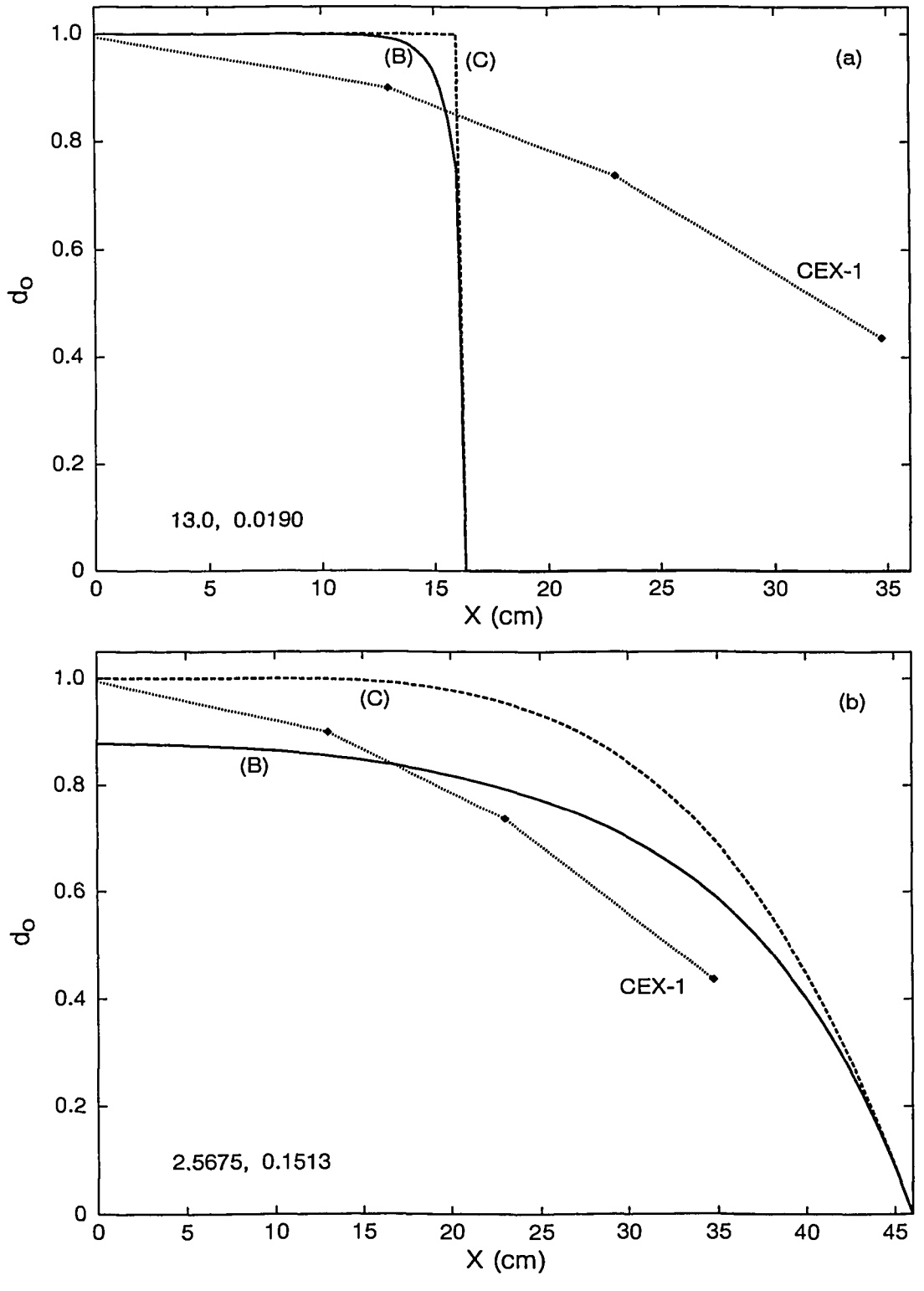

FIGURE 11: Comparison of the local degree of oxidation d_o after 40 months of unlimited air supply for cases (A), (B) and (C) of the oxygen-consumption-rate dependence on d_o (cf. Equations (76) and (77)) with the part of the CEX-1 oxidation profile of Figure 10 (shown by dotted line) that lies to the right of the defect (between the defect and

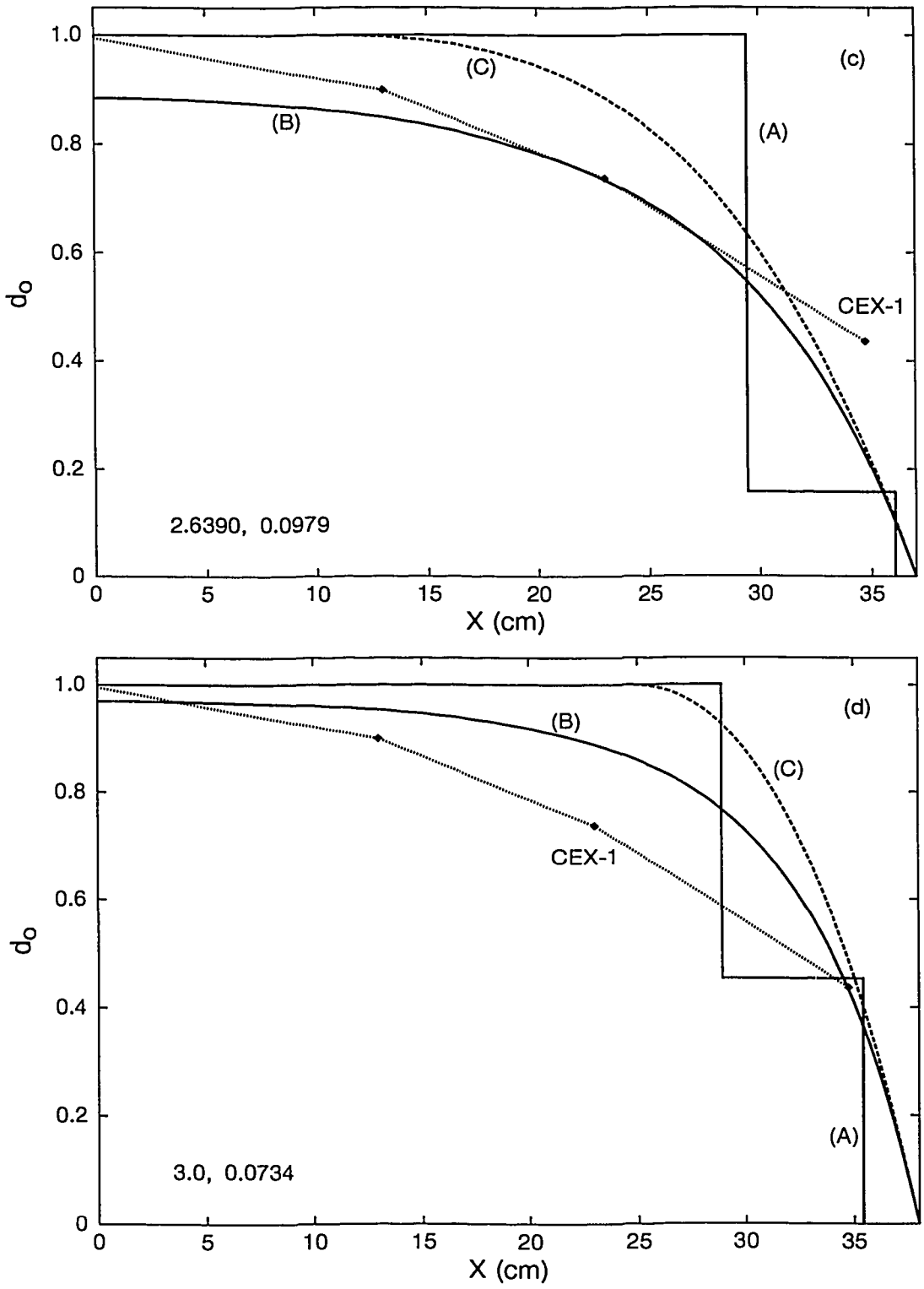

FIGURE 11 cont'd: the farther end of the fuel element). The individual plots are labeled in the lower left corner by the respective values of K_{v0} (in $10^{-9}\text{mol} \cdot \text{cm}^{-3} \cdot \text{s}^{-1}$) and D_e (in $\text{cm}^2.\text{s}^{-1}$).

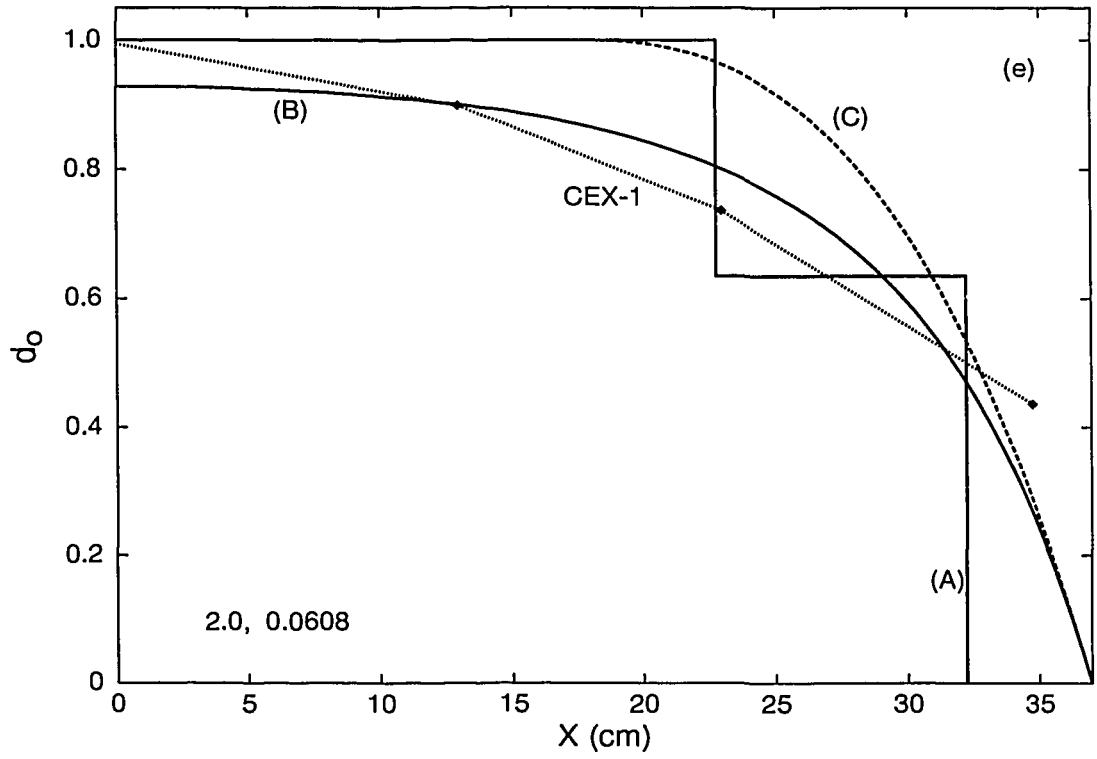

FIGURE 11 continued

Note that to achieve reasonable agreement between theory and experiment, one has to use the parameters that give for X_{max} of Equation (33) the values of 20 to 23 cm. This is much larger than what was obtained from the limited-air data of the second storage period. One should not be bothered very much by this fact in the light of the uncertainties related to the interpretation of the limited-air data. Clearly, greater weight should be given to the comparison with the unlimited-air data. It is also possible that tails of the oxidized region in the second CEX-1 storage period extended as far as 20 cm from the defect, but the degree of oxidation beyond 5 cm was too small to be registered during the second CEX-1 examination. Quite reasonable agreement between theory and experiment is obtained in Figures 11c,d,e with $K_{v0} \approx 2.0 \times 10^{-9}$ to 3.0×10^{-9} mol $\cdot$ cm$^{-3} \cdot$ s^{-1} and $D_e \approx 0.06$ to 0.1 cm$^2 \cdot$ s^{-1}. These values of the consumption rate are larger by less than one order of magnitude than the value used by Garisto [3], but they are in good agreement with all available experimental data. The value of D_e is much larger than that obtained from the comparison with the limited-air data, and it corresponds to a rather low, realistic value of tortuosity, $\tau \approx 1.9$ to 2.5. Starting from the CEX-1 data, the value of D_e is directly proportional to X_{40}^2 (cf. Equations (75) and (33)), and the value of K_{v0} is then determined by the shape of the d_o curves. Because the rather different models that we consider in this report give practically identical parabolic law of the advance of the oxidation front (cf. Equations (71), (75) and (88)), one can assume that this parabolic law is an essential attribute of the diffusion process independent of the details of the reaction taking place. Thus this determination of D_e may be a rather reliable one. In Figure 11, the shape of the

experimental d_0 curve resembles that obtained with the (B) and(C) model dependence of k on d_o. In view of the simplicity of the equivalent porous medium model, the agreement between the experimental and theoretical (B) and (C) d_o curves is encouraging. One can hope that a variation of the (B) and (C) cases, perhaps along the line of Section 3.4, can lead to a good description od the used fuel oxidation.

5. CONCLUSIONS

Using the integral method, we have solved in an exhaustive way the zero-order reaction-diffusion model with a constant consumption rate, and limited and unlimited oxygen supply. In Section 2.4 a rigorous treatment of the effect of the dependence of the consumption rate on the local degree of oxidation was presented, which is relevant to the third unlimited-air-supply storage period of the CEX-1 experiment. We have verified that the quasi-steady-state approximation used for the limited-oxygen-supply case in Ref. [3] is justified for parameter values applicable to the CEX-1 experiment. We have found plausible values for the consumption rate and apparent diffusivity that give good agreement, especially with the CEX-1 unlimited-air-supply data. Further experimental work is desirable to verify whether these values correspond to reality.

Some diffusion-controlled oxidation models were also studied in Section 3. For unlimited oxygen supply in the linear geometry we found an exact solution. This solution provides a good approximation for the spherical geometry. This result sheds some light on the origin of the oxygen consumption rate used in the reaction-diffusion models of Section 2, and can be useful for correct interpretation of experiments on the oxidation of individual UO_2 grains (or powders and fragments).

We have found that the temporal advance of the oxidation front is essentially independent of the details of the models, at least for models investigated in this report, and that it is given by a parabolic law.

More theoretical work needs to be done on the topics of Sections 3.2, 3.3, and 3.4, especially on Section 3.4 where an initial formulation of an improved reaction-diffusion model incorporating the results for the diffusion-controlled oxidation of the grains of Section 3.3 is given.

In summary, although some old questions have been at least partly answered in this report, a few new questions were opened.

ACKNOWLEDGEMENTS

The work described in this report was funded jointly by AECL and Ontario Hydro under the CANDU Owners Group (COG) program.

I would like to thank K. M. Wasywich, R. McEachern and P. Taylor for helpful

discussions, for providing the data for Figure 10 and encouraging me to complete the relevant analysis of Section 2.4 (KMW), and PT, KMW and J. Freire-Canosa for reviewing the report.

REFERENCES

[1] I. E. Oldaker. 1979. The WNRE Program to Investigate the Stability of Irradiated CANDU Power-Reactor Fuel under Dry Storage Conditions. Atomic Energy of Canada Limited Report, AECL-6431.

[2] K. M. Wasywich, W. H. Hocking, D. W. Shoesmith, and P. Taylor. 1993. Differences in Oxidation Behavior of Used CANDU Fuel During Prolonged Storage in Moisture-Saturated Air and Dry Air at 150°C. Nuclear Tech. **104**, 309.

[3] F. Garisto. 1993. Modelling the Oxidation of Defected Fuel Elements. Atomic Energy of Canada Limited Report, AECL-10734.

[4] T. R. Goodman. 1958. The Heat-Balance Integral and Its Application to Problems Involving a Change of Phase. ASME Transactions **80**, 335.

[5] T. R. Goodman. 1964. Application of Integral Methods to Transient Nonlinear Heat Transfer. Advances in Heat Transfer (T. F. Irwin and J. P. Hartnett, Eds., New York: Academic Press) **1**, 51.

[6] J. Crank and R. S. Gupta. 1972. A Moving Boundary Problem Arising from the Diffusion of Oxygen in Absorbing Tissue. J. Inst. Maths. Applics. **10**, 19.

[7] K. M. Wasywich. 1993. Characteristics of Used CANDU Fuel Relevant to the Canadian Nuclear Fuel Waste Management Program. Atomic Energy of Canada Limited Report, AECL-10463.

[8] K. M. Wasywich, J. D. Chen, C. R. Frost, and J. Freire-Canosa. 1984. Long-Term Behaviour of Irradiated CANDU Fuel in Concrete Canister Storage – Test Results. *In* Irradiated Fuel Storage: Operating Experience and Development Programs, Toronto, Ontario, 1984, 393.

[9] J. Crank. 1957. Mathematics of Diffusion, Oxford at the Clarendon Press, p. 117.

[10] S. Aronson, R. B. Roof, Jr., and J. Belle. 1957. Kinetic Study of the Oxidation of Uranium Dioxide. J. Chem. Phys. **27**, 137.

[11] R. E. Einziger and R. E. Woodley. 1985. Low Temperature Spent Fuel Oxidation under Tuff Repository Conditions. *In* Proc. Waste Management 1985, Tuscon, Arizona, March 24-28. Vol. **1** (Ed. R. G. Post, Arizona Board of Regents), 505.

[12] R. E. Woodley, R. E. Einziger, and H. C. Buchanan. 1989. Measurement of the Oxidation of Spent Fuel between 140 and 225°C. Nuclear Tech. **85**, 74.

[13] K. B. Alberman and J. S. Anderson. 1949. The Oxides of Uranium. J. Chem. Soc. Suppl. No. **2**, S303.

[14] H. R. Hoekstra, A. Santoro, and S. Siegel. 1961. The Low Temperature Oxidation of UO_2 and U_4O_9. J. Inorg. Nucl. Chem. **18**, 166.

[15] I. J. Hastings, D. H. Rose, J. R. Kelm, D. A. Irvine, and J. Novak. 1986. Air Oxidation of UO_2 Fuel Fragments at 175° to 400 °C. Commun. Amer. Ceramic Society **69** [2], C-16.

[16] L. E. Thomas, R. E. Einziger, and H. C. Buchanan. 1993. Effect of Fission Products on Air-Oxidation of LWR Spent Fuel. J. Nucl. Materials **201**, 310.

[17] J. S. Anderson, L. E. J. Roberts, and E. A. Harper. 1955. The Oxides of Uranium. Part VII. The Oxidation of Uranium Dioxide. J. Chem. Soc., 3946.

[18] D. E. Y. Walker. 1965. The Oxidation of Uranium Dioxides. J. Appl. Chem. **15**, 128.

[19] J. Novak, I. J. Hastings, E. Mizzan, and R. J. Chenier. 1983. Postirradiation Behaviour of UO_2 Fuel I: Elements at 220 to 250°C in Air. Nuclear Tech. **63**, 254.

[20] L. E. Thomas and R. E. Einziger. 1992. Grain Boundary Oxidation of Pressurized-Water Reactor Spent Fuel in Air. Materials Characterization **28**, 149.

[21] T. K. Campbell, E. R. Gilbert, C. K. Thornhill, and B. J. Wrona. 1989. Oxidation Behavior of Spent UO_2 Fuel. Nuclear Tech. **84**, 182.

[22] R. McEachern, Personal communication.

[23] P. Taylor, Personal communication.

APPENDIX A

The MAPLE V Program Used in Section 2.4

```
# Usage: for example:
# restart; n:=5; Plateau:=true; Brute:=true; Digits:=20;
#          read 'this_file_name';
#

# This Maple V program finds the ordinary differential equations for the
# integral-method approximation of order  n  to the 1D diffusion-reaction
# (oxidation) problem with zero-order reaction in O concentration,
# unlimited oxygen supply, and consumption rate dependending on the
# degree of oxidation.
# It also finds the values of gamma'i (plateaus) for the (A) case
# (Plateau:=true), and the asymptotic behaviour for the (B) and (C)
# cases (Asymp:=true).

# Here  a.i  represents  a'i  with an overbar.

printlevel:=0:

if(Plateau=true) then Asymp:=false; fi;
if(not type(Asymp,boolean)) then Asymp:=true; fi;
Plateau:=not Asymp;
if(Plateau=true and not type(Brute,boolean)) then Brute:=false; fi;

if(n<4) then

 print('n  must be >= 4 !!!');

else

 n2:=n-2:
 n1:=n-1:
 n3:=n-3:
 # From boundary conditions:
 a.n2 := t -> 1/2*(xm(t)^2-n1*(n+n2*a1(t))
- sum('(n-i)*(n1-i)*a.i(t)','i'=2..n3));
 a.n1 := t -> -n-2*a.n2(t)-sum('(n-i)*a.i(t)','i'=1..n3);
 a.n := t -> -1 - a.n1(t) - a.n2(t) - sum('a.i'(t),'i'=1..n3);
 # Test boundary conditions (the following 3 expressions should give 0):
 lprint('  ',radsimp(1+sum('a.i(t)','i'=1..n)));
 lprint('  ',radsimp(sum('i*a.i(t)','i'=1..n)));
```

```
lprint('  ',radsimp(sum('i*(i-1)*a.i(t)','i'=2..n)-xm(t)^2));
# D3 in the equation for diff(xm(t),t):
D3 := radsimp(sum('i*(i-1)*(i-2)*a.i(t)','i'=3..n));
print('D3' = D3/xm(t)^3);
# Integral condition (0th moment; k=0):
Eset:={sum((diff('a.i'(t),t)*xm(t)-'i'*'a.i'(t)*diff(xm(t),t))/('i'+1),
       'i'=1..n)+ a1(t)/xm(t)+xm(t)-FiCase0 = 0}:
# Higher moment conditions, k=1..n-4:
n4:=n-4;
for k from 1 to n4 do
  Eset := Eset union
        {sum((diff('a.i'(t),t)*xm(t)-'i'*'a.i'(t)*diff(xm(t),t))
              /('i'+k+1), 'i'=1..n)
         + k*sum('i'/('i'+k-1)*'a.i'(t)/xm(t),'i'=1..n)
         + (xm(t)-FiCase.k/xm(t)^k)/(k+1) = 0};
od;
SubsS := {diff(xm(t),t)=Dxm,seq(diff(a.i(t),t)=Da.i,i=1..n3)};
Eset := subs(SubsS,Eset);
Vset := {seq(Da.i,i=1..n3)};
# Calculate RHS of equations for diff(a.i(t),t) = Da.i:
RHS := solve(Eset,Vset):
# Check solution:
lprint('   Solution check:', radsimp(subs(RHS,Eset)));
# Assign solutions:
assign(RHS);
for i from 1 to n3 do
       Da.i := collect(Da.i,[Dxm,xm(t)],recursive);
       if(Asymp) then print(evaln(Da.i) = Da.i); fi;
od;

if(Plateau) then
  # Plateaus for the A case:
  printlevel := 0;
  Dxm := 0;
  FiCase0 := 'gami_1'*sqrt(2);
  for k from 1 to n4 do FiCase.k := FiCase.(k-1) * FiCase0; od;
  i := 'i';
  SubsS := {xm(t)=gami*sqrt(2),seq(a.k(t)=a.k.i,k=1..n3)};
  Eset := subs(SubsS,Vset) union {subs(SubsS,D3)};
  Vset := {seq(a.k.i,k=1..n3),gami};

  if(Brute) then
    # By "brute force", the beginning of the sequence of  gami
    # can be obtained in the following way:
    gami_1:=1.;
```

```
    for i from 2 to 10 do
    Eseti:=Eset;
    sol:=solve(Eseti,Vset);
    Nsol := nops({sol});
    for k from 1 to n2 do
       if(op(1,op(k,sol[1]))=evaln(gami)) then break; fi; od;
    g1:=op(2,op(k,sol[1]));
    if(Nsol = 2) then
      for k from 1 to n2 do
         if(op(1,op(k,sol[2]))=evaln(gami)) then break; fi; od;
      g2:=op(2,op(k,sol[2]));
      if(g1 < 0) then
         if(g2 < 0) then print('Both roots are negative'); break; fi;
         gami_1:=g2;
      else
         if(g2 > 0) then print('Both roots are positive'); break; fi;
         gami_1:=g1;
      fi;
    else
      print(Nsol,' solutions: ',g1);
      for s from 2 to Nsol do
        for k from 1 to n2 do
           if(op(1,op(k,sol[s]))=evaln(gami)) then break; fi; od;
        g2:=op(2,op(k,sol[s]));
        print('             ',g2);
        if(g2 > g1) then g1:=g2; fi;
      od;
      gami_1:=g1;
    fi;
    print(i,gami_1,evalf(sqrt(i),10));
    od;
  fi;

  # Recursive equation for  gami  in terms of  gami_1  is thus very
  # simple, it is:
  gami_1:='gami_1';
  sol := solve(Eset,Vset);
  for k from 1 to n2 do
        if(op(1,op(k,sol))=evaln(gami)) then break; fi; od;
  print('The resursion is: ',op(k,sol));
fi;

if(Asymp) then
  #printlevel:=2;
  #Asymptotic behaviour for the B,C cases:
```

```
   SubsS := {Dxm = xi,xm(t)=xi*t,seq(a.k(t)=al.k*t^2,k=1..n3),
     FiCase0=xi*t, seq(FiCase.k=(xi*t)^(k+1),k=1..n4)};
   Eset := {};
   for k from 1 to n3 do
        Da.k := subs(SubsS,Da.k);
        Eset := Eset union {2*al.k = limit(Da.k/t,t=infinity)};
   od;
   Vset := {seq(al.k,k=1..n3)};
   print(op(solve(Eset,Vset))):
 fi;

fi;

#end;
```

Cat. No./N° de cat.: CC2-11174E
ISBN 0-662-16080-3
ISSN 0067-0367

To identify individual documents in the series, we have assigned an AECL-number to each. Please refer to the AECL-number when requesting additional copies of this document from:

Scientific Document Distribution Office (SDDO)
AECL
Chalk River, Ontario
Canada K0J 1J0

Fax: (613) 584-1745 Tel.: (613) 584-3311
ext. 4623

Price: B

Pour identifier les rapports individuels faisant partie de cette série, nous avons affecté un numéro AECL-à chacun d'eux. Veuillez indiquer le numéro AECL-lorsque vous demandez d'autres exemplaires de ce rapport au

Service de distribution des documents officiels (SDDO)
EACL
Chalk River (Ontario)
Canada K0J 1J0

Fax: (613) 584-1745 Tél.: (613) 584-3311
poste 4623

Prix: B